JAMES | Journal of Advances in Modeling Earth Systems

RESEARCH ARTICLE
10.1029/2023MS004094

Toward Fine Horizontal Resolution Global Simulations of Aerosol Sectional Microphysics: Advances Enabled by GCHP-TOMAS

Betty Croft[1,2], Randall V. Martin[2], Rachel Y.-W. Chang[1], Liam Bindle[2], Sebastian D. Eastham[3,4], Lucas A. Estrada[5], Bonne Ford[6,7], Chi Li[2], Michael S. Long[8,9], Elizabeth W. Lundgren[5], Saptarshi Sinha[2], Melissa P. Sulprizio[5], Yidan Tang[2], Aaron van Donkelaar[2], Robert M. Yantosca[5], Dandan Zhang[2], Haihui Zhu[2], and Jeffrey R. Pierce[6]

[1]Department of Physics and Atmospheric Science, Dalhousie University, Halifax, NS, Canada, [2]McKelvey School of Engineering, Washington University in St. Louis, St. Louis, MO, USA, [3]Laboratory for Aviation and the Environment, Massachusetts Institute of Technology, Cambridge, MA, USA, [4]Now at Faculty of Engineering, Department of Aeronautics, Imperial College London, London, UK, [5]Harvard John A. Paulson School of Engineering and Applied Sciences, Harvard University, Cambridge, MA, USA, [6]Department of Atmospheric Science, Colorado State University, Fort Collins, CO, USA, [7]Now at Cooperative Institute for Research in the Atmosphere (CIRA), Colorado State University, Fort Collins, CO, USA, [8]NASA Goddard Space Flight Center, Global Modeling and Assimilation Office (GMAO), Greenbelt, MD, USA, [9]Science Systems and Applications, Inc., Lanham, MD, USA

Key Points:

- We couple aerosol microphysics with GEOS-Chem's High-Performance configuration for fine (25 km × 25 km) global-resolution capability
- Global-mean aerosol number increases with model resolution, dominated by particles smaller than 10 nm in the over-ocean free troposphere
- Toward finer horizontal resolution, enhanced particle precursor loading in the free troposphere promotes particle formation and growth

Supporting Information:

Supporting Information may be found in the online version of this article.

Correspondence to:

B. Croft,
betty.croft@dal.ca

Citation:

Croft, B., Martin, R. V., Chang, R. Y., Bindle, L., Eastham, S. D., Estrada, L. A., et al. (2024). Toward fine horizontal resolution global simulations of aerosol sectional microphysics: Advances enabled by GCHP-TOMAS. *Journal of Advances in Modeling Earth Systems*, *16*, e2023MS004094. https://doi.org/10.1029/2023MS004094

Received 25 OCT 2023
Accepted 22 SEP 2024

Abstract

Global modeling of aerosol-particle number and size is important for understanding aerosol effects on Earth's climate and air quality. Fine-resolution global models are desirable for representing nonlinear aerosol-microphysical processes, their nonlinear interactions with dynamics and chemistry, and spatial heterogeneity. However, aerosol-microphysical simulations are computationally demanding, which can limit the achievable global horizontal resolution. Here, we present the first coupling of the TwO-Moment Aerosol Sectional (TOMAS) microphysics scheme with the High-Performance configuration of the GEOS-Chem model of atmospheric composition (GCHP), a coupling termed GCHP-TOMAS. GCHP's architecture allows massively parallel GCHP-TOMAS simulations including on the cloud, using hundreds of computing cores, faster runtimes, more memory, and finer global horizontal resolution (e.g., 25 km × 25 km, 7.8×10^5 model columns) versus the previous single-node capability of GEOS-Chem-TOMAS (tens of cores, 200 km × 250 km, 1.3×10^4 model columns). GCHP-TOMAS runtimes have near-ideal scalability with computing-core number. Simulated global-mean number concentrations increase (dominated by free-tropospheric over-ocean sub-10-nm-diameter particles) toward finer GCHP-TOMAS horizontal resolution. Increasing the horizontal resolution from 200 km × 200–50 km × 50 km increases the global monthly mean free-tropospheric total particle number by 18.5%, and over-ocean sub-10-nm-diameter particles by 39.8% at 4-km altitude. With a cascade of contributing factors, free-tropospheric particle-precursor concentrations increase (32.6% at 4-km altitude) with resolution, promoting new-particle formation and growth that outweigh coagulation changes. These nonlinear effects have the potential to revise current understanding of processes controlling global aerosol number and aerosol impacts on Earth's climate and air quality.

Plain Language Summary

Small particles in the air have important effects on Earth's climate and air quality. Representing the number and size of these particles in global models is challenging because their processes are complex. This factor has often limited global-model horizontal resolution because fine global resolution models (e.g., 25 km × 25 km or smaller) generally ran too slowly but would be useful for representing details missed at traditional coarse resolution (e.g., 200 km × 250 km). We start with a detailed particle scheme that previously only ran at coarse global resolution because fine resolution would take too long. We present the initial use of this scheme in an updated model version, with a structure allowing a fast-running, high-memory model with fine resolution, by using hundreds to thousands of computer cores. In the updated structure, model speed increases with the number of cores used. We find that the total number of particles in the model is more with fine compared to coarse model resolution. These increases are most in Earth's remote regions and for particles which come from gas. Using fine model resolution globally when representing particles could change our understanding of how they impact Earth's climate and air quality.

1. Introduction

Aerosol particles and their associated microphysical processes have a key influence on Earth's air quality and climate. Many of the aerosol microphysical processes that control particle number and size are strongly nonlinear (Cai et al., 2022; Kerminen et al., 2004, 2018; Zaidan et al., 2018). Aerosol microphysical processes include new particle formation from precursor vapors (Almeida et al., 2013; Dunne et al., 2016; Kirkby et al., 2011; Riccobono et al., 2014) and particle growth by coagulation and vapor condensation (Fuchs, 1964; Pierce et al., 2011, 2015; Ramnarine et al., 2019; Riipinen et al., 2011), with new particle formation and coagulation being strongly nonlinear. Aerosol microphysical processes are climate relevant since particle number and size are key controls on aerosol direct scattering and absorption of incoming solar radiation (Charlson et al., 1987). Furthermore, particle number and size influence cloud properties, including reflectivity and lifetime, since aerosols act as the seeds for cloud droplet and ice crystal formation, affecting cloud microphysical processes that are of key importance for cloud radiative effects (Albrecht, 1989; Bellouin et al., 2020; IPCC, 2023; Twomey et al., 1984). While these effects were identified decades ago, their quantification remains highly uncertain due to a variety of challenges related to clouds, aerosols and their interactions, including the representation of complex and nonlinear aerosol microphysical processes in global models (Myhre et al., 2013; Regayre et al., 2018). Furthermore, by influencing aerosol size distributions, aerosol microphysical processes influence the mass of atmospheric particulate matter that is at sizes that affect human morbidity and mortality (e.g., diameters smaller than 2.5 μm, $PM_{2.5}$) (Cohen et al., 2017). As a result, aerosol microphysical processes play a key role in controlling the habitability of Earth's environment and as such their representation is important, though challenging for global atmospheric models.

Fine global model horizontal resolution is desirable to represent the spatial details of aerosol geographic distributions. However, the movement toward finer global model spatial resolution has been challenging for size-resolved aerosol microphysical simulations because of the strong computational demands associated with adding significantly more tracers and processes to models (Adams & Seinfeld, 2002; Mann et al., 2014; Matsui, 2017; Tegen et al., 2019; F. Yu & Luo, 2009; Zaveri et al., 2021). As a result, global models may default to assumed sizes for parameterizations requiring aerosol size information, leading to a range of uncertainties in model output (Jin et al., 2019; J. Li et al., 2015). These uncertainties make more detailed aerosol size-resolved schemes a preferable option (e.g., Matsui & Mahowald, 2017) if their computational demands can be satisfied. The computational demands of aerosol microphysical schemes can be reduced by improving the efficiency of size-resolved schemes (Y. H. Lee & Adams, 2012; Pierce & Adams, 2009). However, there are associated losses in model fidelity, such as a requirement for reductions in the aerosol size-bin resolution. In response to these challenges, we present recent advances that enable finer global horizontal resolution for size-resolved aerosol microphysical simulations with the GEOS-Chem model (www.geos-chem.org) (GEOS-Chem, 2024).

The approach we use here for dealing with the challenge of high computational demands is to speed up simulation runtimes by massive parallelization, which enables simulations on 100–1,000s of cores. This multi-node capability was introduced to the GEOS-Chem model with the development of the GEOS-Chem High-Performance (GCHP) configuration (Eastham et al., 2018). Recently, GCHP has been further developed with improvements to advection, resolution, performance and accessibility (Martin et al., 2022), including stretched-grid capability for fine resolution over user-specified regions (Bindle et al., 2021). GCHP's near-ideal scalability between runtimes and employed computing nodes is well suited to the computational demands of size-resolved aerosol microphysics schemes. The previous inability to use more than one computing node has been an even greater limitation for more complex simulations (such as with size-resolved aerosol microphysics), which require more memory and computation per grid cell than the standard GEOS-Chem (bulk aerosol) model. Here, we use GCHP to address this challenge.

In this study, we use the TwO-Moment Aerosol Sectional (TOMAS) scheme (Adams & Seinfeld, 2002; Kodros & Pierce, 2017). We present the first implementation of TOMAS in GCHP, which enables finer horizontal resolution simulations (approximately 25 km × 25 km globally) than were previously possible with the "classic" single-node GEOS-Chem framework, which limited TOMAS simulations to at most 2° × 2.5° globally. We also develop this capability on the cloud for broader community accessibility. We use the GCHP-TOMAS configuration to explore the horizontal-resolution dependency of simulated size-resolved aerosol number concentrations and aerosol microphysical process rates in a global model. Such study has been limited to date due to the computational demands of size-resolved aerosol microphysics schemes like TOMAS. This study aims to address this knowledge gap.

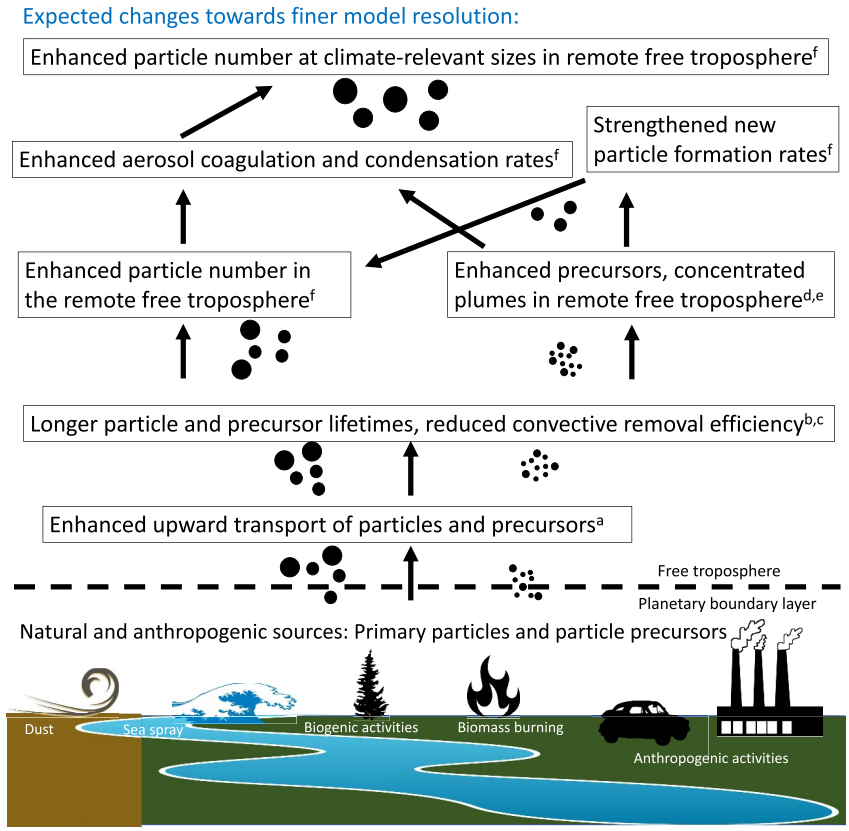

Figure 1. Schematic of expected changes toward finer horizontal resolution and impacting simulated free-tropospheric particle number concentrations in the GEOS-Chem High-Performance configuration with the Two Moment Aerosol Sectional scheme (GCHP-TOMAS). Expected changes are in boxes. As illustrated on the schematic, previous studies have identified and examined several relevant drivers at work in the GEOS-Chem model and its associated meteorology, including: [a]K. Yu et al. (2018) (upward transport strengthens due to less spatial and temporal averaging-out of transient vertical motions toward finer resolution); [b]Croft et al. (2014); [c]Williamson et al. (2019) (lifetimes lengthen with injection to higher altitudes, reduced convective wet removal efficiency toward finer resolution); [d]Eastham and Jacob (2017); [e]Zhuang et al. (2018) (increased concentrations in transport plumes and reduced numerical diffusion toward finer resolution); [f]examined in this study.

Toward finer resolution, our global-model aerosol simulations have a spatial-resolution dependency, which can arise from an expected cascade of factors as illustrated in Figure 1. Using archived meteorological fields with no feedback between the aerosols and the meteorology (termed as offline meteorology), K. Yu et al. (2018) found a strengthening of upward transport when GEOS-Chem model resolution was increased from 2° × 2.5°–0.25° × 0.3125°, yielding up to 40% enhancement in free-tropospheric tracer concentrations. The strengthening vertical transport toward finer model resolution is due to better retention of transient vertical motions, which are important for upward transport but are averaged out toward coarser resolution. Toward finer (increased) resolution, strengthened vertical transport injects aerosols and their precursors to higher altitudes than at coarse resolution. Aerosol lifetimes lengthen with increasing injection height; as previously shown with the GEOS-Chem model (Croft et al., 2014). Additionally, in the absence of separate in-cloud and clear-sky tracers (such as in the GEOS-Chem model), convective wet removal is less efficient toward finer horizontal resolution (Williamson et al., 2019). These factors contribute to enhanced particle and precursor mass loading in the free troposphere as resolution increases. Furthermore, using GEOS-Chem and its dynamical core, previous studies have shown that numerical diffusion weakens toward finer model resolution, leading to weaker chemical plume dilution and higher in-plume concentrations (Eastham & Jacob, 2017; Zhuang et al., 2018). Working from these known effects of horizontal resolution on GEOS-Chem simulations, we use the newly developed GCHP-TOMAS model to explore the impacts of model horizontal resolution on rates of new particle formation, particle-precursor condensation, and coagulation; as well as on size-resolved aerosol number concentrations (upper portion of Figure 1).

Resolution dependency, arising from nonlinear aerosol process rates, dynamics and chemistry, remains as one of the key challenges in accurately representing aerosol particles and their microphysical processes in global models (e.g., Paolella et al., 2018; D. Zhang et al., 2023). In many global models, coarse resolution has been shown to lead to systematic biases in parameterizations of nonlinear aerosol processes and emissions when scales of variability are finer than the model resolution (Goto et al., 2020; S. S. Lee et al., 2018; Meng et al., 2021; Pierce et al., 2009; Wainwright et al., 2012; Weng et al., 2020). As well, model-spatial-resolution effects due to nonlinear process rates have also been identified for a variety of gas-phase atmospheric pollutants and their emissions (e.g., C. Li et al., 2023; Long et al., 2014; Zakoura & Pandis, 2018). The dependency on resolution has motivated movement in recent years toward progressively finer spatial resolution in global and regional models (e.g., Dinkelacker et al., 2022; Feng et al., 2021; Goto et al., 2020; Hu et al., 2018; Keller et al., 2021; Sato et al., 2016). Motived by these concerns, here we explore the impacts of horizontal resolution on size-resolved aerosol microphysics simulations at a finer global resolution than previously possible.

In the following sections, we provide a description of the GCHP-TOMAS configuration. We present timing tests that characterize the simulation runtimes as a function of the number of computational cores used, for a range of global model horizontal resolutions from about 25 km × 25 km (termed C360) to about 400 km × 400 km (termed C24). The nomenclature CN is used to identify the horizontal grid resolution, where N is the number of grid boxes along each edge of the six faces of the model's cubed sphere grid (Martin et al., 2022). We then examine the global distribution of monthly mean aerosol number and size simulated by GCHP-TOMAS at a fine global resolution (about 50 km × 50 km, termed C180) relative to a coarse global resolution simulation (about 200 km × 200 km, termed C48). We quantify differences in size-resolved particle number concentrations and process rates between these resolutions to understand the horizontal resolution dependency of these size-resolved aerosol microphysics simulations with GCHP-TOMAS.

2. Model Description

GEOS-Chem (www.geos-chem.org) (GEOS-Chem, 2024) is an atmospheric chemistry model first described by Bey et al. (2001), which can be driven both online in weather and climate models, and offline using archived meteorology. GEOS-Chem is a grid-independent model (Long et al., 2015) and has been coupled to a variety of meteorological and climate models (Feng et al., 2021; Hu et al., 2018; Keller et al., 2021; Lin et al., 2020; Lu et al., 2020; Murray et al., 2021). For this study, we employed the Modern-Era Retrospective analysis for Research and Applications, Version 2 (MERRA-2) reanalysis meteorology, which is available from 1980 to present at 0.5° × 0.625° spatial resolution (Gelaro et al., 2017). MERRA-2 is available from the Goddard Earth Observation System (GEOS) of the NASA Global modeling and Assimilation Office (GMAO). With the offline use of MERRA-2, there is no feedback of GEOS-Chem's aerosol-chemistry simulation on the meteorology. The meteorological fields are re-gridded to the horizontal resolution of our simulations, yielding a strengthening of upward transport toward finer resolution (K. Yu et al., 2018). Archived MERRA-2 meteorological fields employed for convective transport are 3-hourly averages and are based on the Relaxed Arakawa-Schubert scheme (Moorthi & Suárez, 1992). The GEOS-Chem model was originally designed to run on a single computational node with tens of cores and in this configuration is called GEOS-Chem-Classic (GCC). Global GCC full-chemistry simulations are limited to resolutions of 2° × 2.5° or 4° × 5° due to memory limitations of a single node and insufficient cores, with the capability for finer spatial resolution over regional domains through the use of boundary conditions from previous coarser resolution global simulations (e.g., K. Li et al., 2021; L. Zhang et al., 2015). The GEOS-Chem model has the capability for size-resolved aerosol microphysics by employing the TwO-Moment Aerosol Sectional (TOMAS) scheme (Adams & Seinfeld, 2002; Kodros & Pierce, 2017; Y. H. Lee & Adams, 2012) or the Advanced Particle Microphysics (APM) model (F. Yu & Luo, 2009). TOMAS is employed for this study and is described later in this section. Previous study with GCC has highlighted the advantages of TOMAS' size-resolved simulations (over GCC without TOMAS) for representation of aerosol properties, for example, as needed for aerosol optical depth (Zhu et al., 2023).

In recent years, the GEOS-Chem model has been developed to have multi-node capability, enabling a single simulation to use 100–1,000s of computational cores (Eastham et al., 2018; Martin et al., 2022; Zhuang et al., 2020). This configuration, termed GEOS-Chem High Performance (GCHP), uses distributed memory parallelization enabled through the Earth System Modeling Framework (ESMF) (Hill et al., 2004) and the Modeling Analysis and Prediction Layer (MAPL) (Suarez et al., 2007). The OpenMP parallelization (used by GCC) is disabled for GCHP, resulting in a pure MPI implementation without any thread parallelization. GCHP

offers GEOS-Chem simulations with faster speed, higher memory and in turn finer global spatial resolution (currently up to about 12 km × 12 km globally for horizontal resolution) than simulations with GCC. GCHP uses a cubed-sphere grid with six faces, which offers accurate and efficient transport simulation due to its more uniform grid boxes, relative to recti-linear latitude-longitude grids. GCHP also offers stretched-grid simulations (Bindle et al., 2021), which provide the option of shrinking the spatial extent of a target face. This process does not change the total number of grid boxes on any of the faces. However, the stretched grid provides regionally finer resolution over the target face (centered over any geographic location), relative to the other 5 faces (that undergo expansion of their total spatial extent). As a result, the computational demands and total number of grid boxes can be unchanged for a stretched grid relative to a globally uniform resolution simulation unless the model timestep is shortened. The recent generation of GCHP (version 13) with improved capabilities for performance, resolution, accuracy, and accessibility (Martin et al., 2022) is employed as the starting point in this study.

In this study, we develop and present the first coupling of the aerosol microphysical scheme TOMAS with GCHP (termed GCHP-TOMAS), using model version 13.3.4 (The International GEOS-Chem User Community, 2021, 2023a, 2023b, 2023c). Additionally, we implement TOMAS in GCHP version 14.2.0 (The International GEOS-Chem User Community, 2023d), which includes updates such as the migration of cloud chemistry to The Kinetic PreProcessor (KPP) chemical solver and additional species for halogen chemistry. GCHP-TOMAS is available as part of the public release of GCHP version 14.3.0 and subsequent public release versions (The International GEOS-Chem User Community, 2024). Prior GCHP versions have not included TOMAS microphysics because additional code developments were required for functionality. TOMAS' grid-independency, which we develop in this study, provides the capability for future coupling of TOMAS with online-meteorology models (for aerosol-meteorology feedbacks). These developments include revisions to TOMAS microphysical rate diagnostics, removal of archaic dependencies on diagnostic frameworks not supported by GCHP, and code architecture for enabling TOMAS as an option in the compilation of GCHP. This new framework also offers the option of stretched-grid simulations with GCHP-TOMAS.

Within the GCHP framework, TOMAS maintains the same functionality as in GCC. TOMAS tracks aerosol number and mass in a set of size bins. For the purposes of this study, we use 13 logarithmically spaced bins spanning particle diameters from 3 nm to 1 μm, with 2 additional size bins from 1 to 10 μm. The prognostic aerosol components considered by TOMAS are sulfate, sea salt, hydrophobic and hydrophilic carbonaceous particles (organic and black carbon), and dust; and the diagnostic components are ammonia and water. Particle formation is treated with a ternary scheme (Napari et al., 2002) scaled by 1×10^{-5} following Westervelt et al. (2013), and a binary scheme in regions of low ammonia (Vehkamaki et al., 2002), with an approximation for particles below 3 nm (Kerminen et al., 2004; Y. H. Lee et al., 2013). The model includes both biogenic and anthropogenic secondary organic aerosol (SOA) (Pai et al., 2020), which contributes to condensational growth of particles as a non-volatile species, in addition to the growth by sulfuric acid condensation. Inter-particle coagulation follows a Brownian coagulation scheme (Fuchs, 1964). Both coagulation and new particle formation are strongly non-linear processes that can be influenced by model resolution. Condensation rates are more linear but can be influenced by changes in availability of precursors due to resolution-dependent upward transport changes. We explore the resolution dependency of these rates in the following sections.

For all simulations presented in this study, we treat emissions and deposition as follows. Emissions are treated with the Harmonized Emissions Component (HEMCO) (Lin et al., 2021). The emissions and meteorological fields are re-gridded by ESMF with an online approach (Ramshaw, 1985) to match the chosen horizontal resolution. We use the Community Emissions Data System (CEDS) version-4 inventory (Hoesly et al., 2018; McDuffie et al., 2020) for global anthropogenic emissions of NO_x, CO, SO_2, NH_3, non-methane VOCs, black carbon, and organic carbon. Emissions inventories are available at similar horizontal resolution as the input meteorological fields. A lognormal distribution is assumed for primary particle emissions, with a geometric standard deviation of 2.0, and mass median diameter of 30 nm for fossil fuel burning and 100 nm for biomass and biofuel burning (Pierce et al., 2007). For our simulations, natural emissions are calculated offline for biogenic volatile organic compounds and sea salt (Jaeglé et al., 2011; Weng et al., 2020), and online for dust (Zender et al., 2003). Biomass burning emissions are from the Global Fire Emissions Database (GFED4s) (Van Der Werf et al., 2017). Simulated aerosol removal from the atmosphere occurs by wet deposition associated with large-scale clouds and as part of the vertical transport in wet convective updrafts (as described in detail in Liu et al. (2001) and Wang et al. (2011, 2014)), and dry deposition has a resistance in series approach (Emerson et al., 2020;

Table 1
Summary of Simulations Conducted

Simulation name	Number of model columns	Number of model vertical levels	Number of days simulated	Approximate grid-box horizontal size
C24	24 × 24 × 6 = 3,456	72	7 days (timing test)	400 km × 400 km
C48	48 × 48 × 6 = 13,824	72	2 months	200 km × 200 km
C90	90 × 90 × 6 = 48,600	72	7 days (timing test)	100 km × 100 km
C180	180 × 180 × 6 = 194,400	72	2 months	50 km × 50 km
C360	360 × 360 × 6 = 777,600	72	7 days (timing test)	25 km × 25 km

Wesely, 1989). Wet and dry removal for gas-phase species are also included in the simulations (Amos et al., 2012).

We conduct simulations at both fine and coarse horizontal resolutions. Table 1 summarizes the simulations conducted. The finest resolution simulation that we conduct with GCHP-TOMAS is C360 (25 km × 25 km grid boxes globally), for a 7-day simulation. For monthly mean comparisons, we use C180 (50 km × 50 km grid boxes, globally) as the fine resolution simulation and C48 (200 km × 200 km grid boxes, globally) as the coarse resolution simulation. Simulations used for monthly mean comparisons have a 1-month spin up period and monthly means presented are for the subsequent month. For this study, we chose to focus on August 2019, which serves as an interesting example month, since the Northern Hemisphere summer is strongly influenced by new particle formation combined with stronger anthropogenic emissions than in the Southern Hemisphere. All simulations use the same 72-level terrain-following hybrid sigma-pressure grid extending from the surface to 0.01 hPa. The thickness of the lowest and thinnest model layer, which we refer to as the "surface layer," is approximately 60 m. Model layers become thicker (to about 500 m) towards the upper troposphere.

Simulations are conducted on the following three computing clusters; Compute1 at Washington University in St. Louis, Stetson at Dalhousie University, and Amazon Web Services (AWS) Elastic Compute Cloud (EC2) with AWS ParallelCluster using the c5n.18xlarge instances. Computing architecture details are provided in Table 2. Our simulations on both the Compute1 and Stetson platforms use an Intel Fortran compiler, IntelMPI and GCHP version 13.3.4. The AWS ParallelCluster platform for this study uses the GNU compiler and OpenMPI; with TOMAS implemented in GCHP version 14.2.0, due to its code updates to enable use of the GNU compiler on AWS. In the following section, we consider the performance of this novel implementation of TOMAS in GCHP, including a demonstration of its cloud-computing capability using AWS.

Table 2
Summary of the Architecture Used to Evaluate GCHP-TOMAS Performance

	Compute1	Stetson	AWS EC2
CPU	Intel® Xeon® Gold 6242	Intel® Xeon® Gold 6154	Intel® Xeon® Platinum 8124M
Physical cores per sockets	16	18	18
Sockets per node	2	2	2
ram per node	394 GB	192 GB	192 GB
Clock speed	2.8 GHz	3.00 GHz	3.00 GHz
Microarchitecture	Skylake	Skylake	Skylake
L2/L3 cache size	8000 K/22000 K	1024 K/25344 K	1024 K/25344 K
Interconnect	Infiniband	Infiniband	AWS EFA
Storage	IBM GFPS	NFS mounted via Infiniband	AWS EBS
GCHP version	13.3.4	13.3.4	14.2.0
Number of tracers	356	356	447
Compiler type	Intel	Intel	GNU
MPI	IntelMPI	IntelMPI	OpenMPI

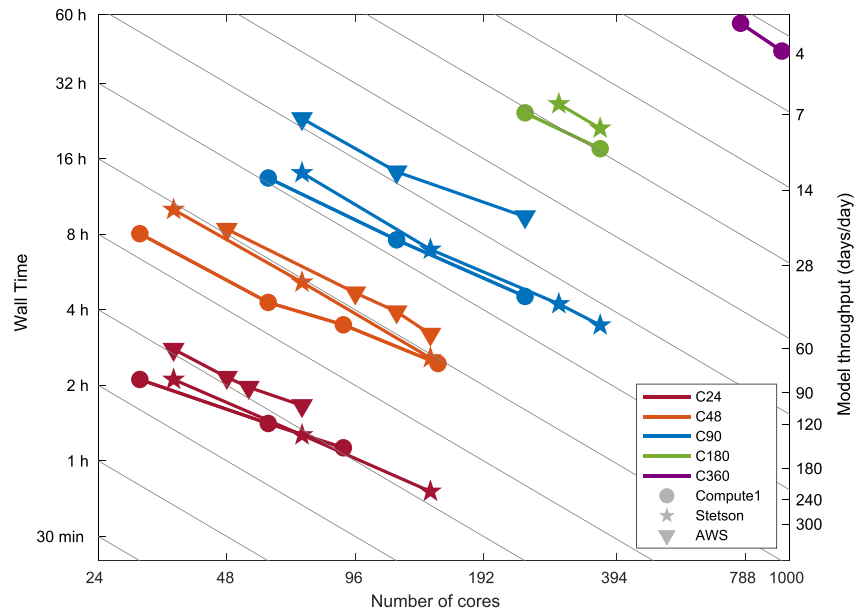

Figure 2. Timing test results for GCHP-TOMAS at variable resolutions (C24, C48, C90, C180, and C360, described in Table 1) on the three platforms (Compute1, Stetson and AWS, described in Table 2). Wall times shown are real-time taken to simulate a 7-day period. Throughput is the number of days simulated for each real-time day. Gray lines indicate ideal scaling.

3. Results and Discussion

3.1. Timing Tests With GCHP-TOMAS

In Figure 2, we show the amount of real time (also referred to as wall time) required to simulate 7-day with the GCHP-TOMAS configuration as a function of the number of computing cores employed. Here, we simulated the period from 1 July 2019 at 00 UTC to 8 July 2019 00 UTC. We use the three computing platforms (Table 2) and various horizontal resolutions (Table 1). The wall times decrease with increasing number of computing cores. We find nearly ideal scalability between core-number tested and wall times at each model resolution (i.e., doubling the number of cores nearly halves the wall times). The lines of ideal scalability are shown in gray on Figure 2. This finding is consistent with the efficient scaling for GCHP found in previous studies (Eastham et al., 2018; Long et al., 2015; Martin et al., 2022).

For these timing tests, our finest resolution simulation (C360, with 55,987,200 grid boxes) has a wall time of about 43 hr when using 960 physical cores (30 nodes). Coarsening the resolution to C180 (13,996,800 grid boxes) or C90 (3,499,200 grid boxes) and using 360 cores enables wall times as low as 16 or 3 hr, respectively. A C24 GCHP simulation on a single Stetson node of 36 physical cores takes about 3 hr, which is similar to the 3 hr for a comparable resolution (4° × 5°) 7-day simulation with the classic GEOS-Chem-TOMAS (GCC-TOMAS) configuration on a single node with 36 physical cores. We find similar results, generally within a factor of two, among the computing clusters and model versions employed for these tests, although the tests on Washington University Compute1 cluster were the fastest of the three, in part due to its newer generation cores with high memory. The AWS EC2 cluster simulations were the slowest. The AWS simulations implemented TOMAS in a more recent GCHP model version that has about 25% more tracers, which added to the computational expense. Further reasons for these differences are examined with Figure 3.

Overall, the GCHP framework enables faster simulations with the TOMAS microphysics relative to the classic single-node GEOS-Chem configuration. Martin et al. (2022) conducted similar timing tests with GCHP without the TOMAS scheme and found wall times that are roughly half of the wall times presented here. This is similar to our finding for wall times of GCC relative to GCC-TOMAS (not shown). However, these speed and memory enhancements from use of more computing cores are sufficient to enable significantly finer global resolution (25 km × 25 km) aerosol microphysics simulations with GCHP-TOMAS than the classic single-node model (GCC-TOMAS), with its limitation of 2° × 2.5° global resolution. Additionally, with the stretched-grid capability

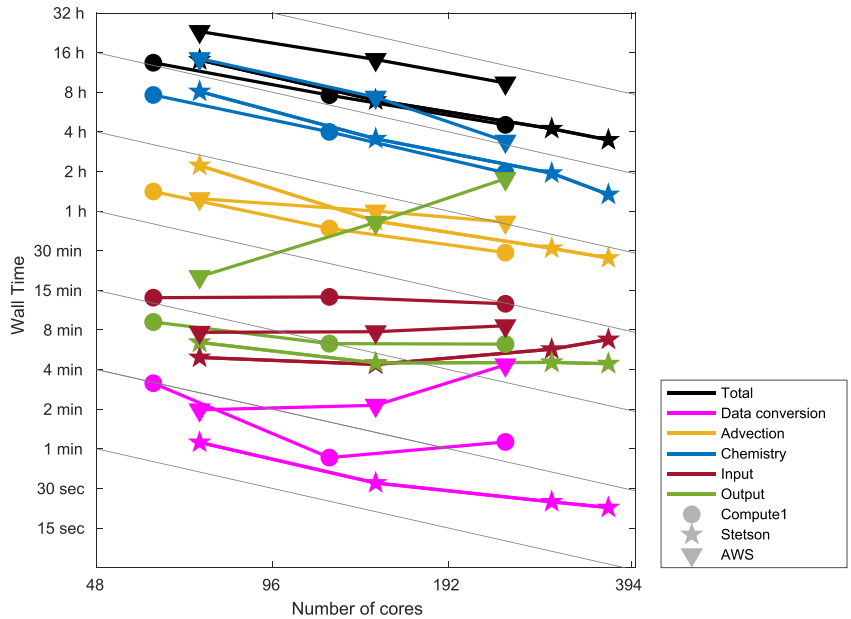

Figure 3. Breakdown of the component-wise contributions to the total wall times as a function of number of cores used for the same timing tests as shown on Figure 2 at C90 resolution on three platforms, Compute1, Stetson and AWS (architecture described in Table 2). Note the different horizontal and vertical scales relative to Figure 2.

of GCHP-TOMAS, finer regional resolution is possible for a similar computational expense relative to a coarser and uniform GCHP-TOMAS global grid with the same total number of grid boxes (not shown).

In Figure 3, we show the relative contributions of the model processes to the timing test total wall times for C90 GCHP-TOMAS simulations as a function of computing core number. Chemistry processes (including aerosol processes with TOMAS) occupy most of the computing time, followed by advection processes. With 360 cores, the chemistry and advection take about 1.5 and 0.5 hr, respectively. We find near ideal scalability for both the chemistry and transport, similar to the result of Martin et al. (2022) for GCHP, except the AWS platform has less than ideal scalability for transport at this resolution with the tested core numbers. Similar scalability issues were noted with GCHP timing tests on AWS when using OpenMPI as opposed to IntelMPI (Zhuang et al., 2018). The input, output and data conversion processes do not scale ideally with the number of computing cores for these tests but occupy a minority of the computing time (less than 0.5 hr for these tests, except up to 2 hr on AWS for output). The latter (green line for AWS on Figure 3) may be addressable with further developments to the file system implementation on AWS (Zhuang et al., 2020). Considering all processes, the total times for C90 GCHP-TOMAS on Compute and Stetson (with 356 advected tracers) are roughly double the times for C90 GCHP without TOMAS (with 220 advected tracers) as presented by Martin et al. (2022) (all with the version 13 series). The slowest times are for the AWS simulation with GCHP-TOMAS in the developmental version for v14.2.0, with 447 advected tracers. Although the different model versions (necessitated by code changes required to use the GNU compiler on AWS), combined with the use of OpenMPI inhibit apples-to-apples comparison between AWS and the other 2 platforms; the results presented here show the current expected range of wall times and scalabilities for GCHP-TOMAS, using a variety of platforms, their setups, and recent model versions. We nonetheless achieve our objective of enabling GCHP-TOMAS on the cloud for increased community accessibility.

3.2. Resolution Dependence of Surface-Layer Monthly Mean Aerosol Number Concentrations

The computational speed and memory afforded by GCHP-TOMAS enables size-resolved aerosol microphysics simulations at finer spatial resolution than have been previously possible with GCC. This finer resolution can impact the microphysical processes that influence the global aerosol number concentrations. We characterize the simulated monthly mean aerosol number concentrations at the finer global resolution (here at C180) and compare with a coarser resolution (C48). C48 has 995,328 grid cells, similar to the 943,488 grid cells of the GCC-TOMAS

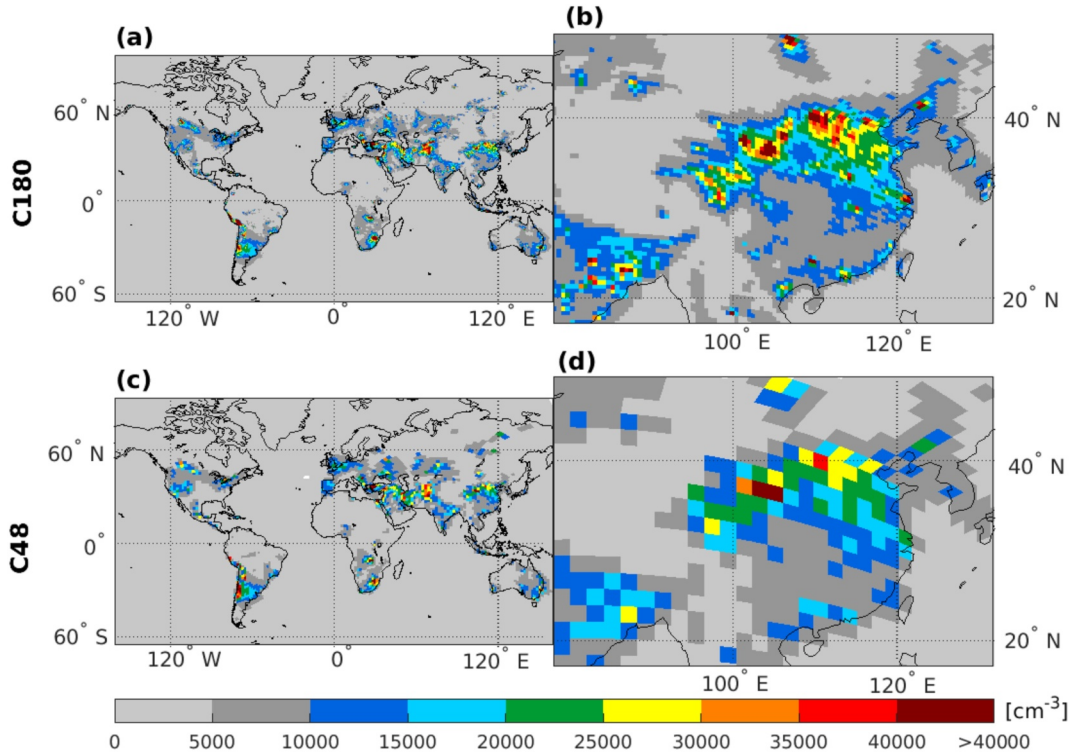

Figure 4. Geographic distribution of simulated monthly mean (August 2019) total particle number concentration (N3, all particles with diameters larger than 3 nm) for the atmospheric layer nearest to Earth surface for GCHP-TOMAS (a) at C180 resolution (about 50 km × 50 km), (b) zoomed-in view over southeast Asia at C180, (c) at C48 resolution (about 200 km × 200 km) and (d) zoomed-in view over southeast Asia at C48.

global limit at 2° × 2.5° and a typical resolution for global aerosol microphysics models. For the remainder of Section 3, we present results from the Stetson platform with TOMAS in GCHP version 13.3.4.

The geographic distribution of the monthly mean (August 2019) surface-layer number concentrations simulated at C180 and C48 with GCHP-TOMAS are shown in Figure 4. The simulations capture the spatial heterogeneity in number concentrations, with enhancements over population centers of the Americas, Europe, Asia, and Africa. The C48 simulation's spatial distribution resembles that of the finer resolution C180 simulation; however, the C180 captures more spatial details than the C48, exemplified by the zoomed-in view of southeast Asia, also shown in Figure 4.

To further examine differences in surface-layer number concentrations between the two resolutions, we re-gridded the C48 to C180 resolution and calculated difference metrics for several particle size ranges. In our study, all re-gridding uses the ESMF conservative (surface-area-weighted) algorithm (https://earthsystemmodeling.org/regrid/, last access: October 2023) (Earth System Modeling, 2023). Table 3 summarizes these global difference metrics for particle number and size in the model layer closest to Earth surface for our C180 relative to C48 GCHP-TOMAS simulations for the August 2019 monthly mean. We define the normalized root mean square difference (NRMSD) as follows:

$$\mathrm{NRMSD} = \frac{\sqrt{\sum_{i=1}^{N} A_i \cdot (C_{h,i} - C_{l,i})^2 / \sum_{i=1}^{N} A_i}}{\sum_{i=1}^{N} A_i \cdot C_{h,i} / \sum_{i=1}^{N} A_i}. \quad (1)$$

All metrics are area-weighted by grid box area (A_i). $C_{h,i}$ and $C_{l,i}$ are the number concentrations at fine (C180, about 50 km × 50 km grid boxes globally) and coarse (C48, about 200 km × 200 km grid boxes globally) horizontal resolution, respectively for the ith of N grid boxes. All metrics are normalized relative to the fine

Table 3
C180 to C48 August 2019 Mean Surface Layer Particle Number Difference Metrics: Normalized Root Mean Square Difference (NRMSD) and Normalized Mean Difference (NMD) as Defined in Equations 1 and 2

	N3[a]	N50[b]	N_10_50[c]	N_sub10[d]
Global				
NRMSD[e] (%)	92.1	56.3	96.3	192.9
NMD[f] (%)	2.0	1.5	0.08	4.8
Ocean				
NRMSD (%)	92.0	35.6	118.2	301.1
NMD (%)	0.8	3.6	−2.3	1.7
Land				
NRMSD (%)	64.2	46.1	66.3	116.0
NMD (%)	2.4	0.2	1.1	5.3

[a]Number of particles with diameters larger than 3 nm. [b]Number of particles with diameters larger than 50 nm. [c]Number of particles with diameters between 10 and 50 nm. [d]Number particles with diameters less than 10 nm. [e]Metrics are defined in the text of Section 3.2 and here refer to the model layer closest to the Earth surface considering global, over-land and over-ocean regions. [f]Positive NMD indicates that C180 has larger concentrations than C48 and negative NMD indicates that C48 has larger concentrations than C180.

resolution simulation, following the methodology of D. Zhang et al. (2023) who presented these metrics for $PM_{2.5}$ concentrations in GCHP. All metrics are multiplied by 100 to obtain a percentage value. The NRMSD is used to consider the degree of spatial heterogeneity since it is sensitive to outliers (D. Zhang et al., 2023). The normalized mean difference (NMD) is defined as below:

$$\mathrm{NMD} = \frac{\sum_{i=1}^{N} A_i \cdot (C_{h,i} - C_{l,i}) / \sum_{i=1}^{N} A_i}{\sum_{i=1}^{N} A_i \cdot C_{h,i} / \sum_{i=1}^{N} A_i}. \quad (2)$$

Here, positive NMD metrics indicate that C180 concentrations exceed C48 concentrations, whereas negative values indicate that C48 concentrations exceed those for C180. The NMD summarizes the global mean change allowing cancellations between positive and negative differences and has less sensitivity to outliers than the NRMSD.

Among the chosen sizes ranges shown on Table 3, the sub-10 nm diameter particles are newly formed (secondary) particles that arise from stable clusters of condensing vapors. The 10–50 nm diameter particles come from newly formed particles that have grown by vapor condensation and coagulation, as well as fresh fossil-fuel and biofuel emissions. The N50 range (number of particles with diameters larger than 50 nm) includes the latter particles that have undergone further growth to diameters of 50 nm and larger, as well as primary particle emissions from a variety of sources, including combustion and wind-driven dust and sea salt. The N50 particles are large enough to affect climate and contain the majority of $PM_{2.5}$. N3 (all particles with diameters larger than 3 nm) includes all the preceding sizes.

The total number (N3) concentrations over the land have a greater NMD of +2.4% than over ocean (+0.8%) for C180 relative to C48 (Table 3), but both are relatively small due to cancellation between regions of increased and decreased number concentration. Since grid-independent sea salt emissions (Weng et al., 2020) are used in our simulations, primary sea-salt emissions do not contribute directly to these differences; although the growth, transport, and removal of these particles can have an influence. The grid-independence capability for dust emissions is the subject of future GCHP-TOMAS developments. The global NMD for N3, considering land and ocean regions together is +2.0%. Again, this modest global NMD for the surface layer arises from cancellations between regions of increased and decreased number concentrations at C180 versus C48, associated with spatial heterogeneity, as further discussed below.

The difference metrics vary with particle size range (Table 3). For the NMD, the greatest enhancement is for the sub-10 nm particles over the land (+5.3%), suggestive of stronger simulated new particle formation (NPF) near the surface layer over land versus over the oceans. Over the oceans, aerosol number concentrations are strongly influenced by particles descending from the free troposphere (e.g., Williamson et al., 2019; Zheng et al., 2018) and NPF is less frequent. We find number concentrations have large NRMSDs between model resolutions, and particularly for oceanic regions (92.0% for total (N3) and 301.1% for sub-10 nm particle number concentrations, between C180 and C48) suggesting considerable spatial heterogeneity. Between these C180- and C48- resolution simulations, the NRMSD increases with decreasing particle size. The sub-10 nm particles have the greatest NRMSDs among size ranges for both over-land and over-ocean regions, reflecting greater spatial heterogeneity toward the smallest particle sizes. The NRMSD that we find here for sub-10 nm particles is considerably larger than D. Zhang et al. (2023) found for $PM_{2.5}$. Contributing mechanisms are explored in the following sections.

3.3. Resolution Dependence of Free-Tropospheric Monthly Mean Aerosol Number Concentrations

The geographic distributions of monthly mean (August 2019) total number (N3) concentration at C180 resolution in the free troposphere at about 4 km altitude (20th model level) and the differences between C180 and C48 resolution are shown in Figure 5. There are more positive than negative differences for the fine- (C180) versus

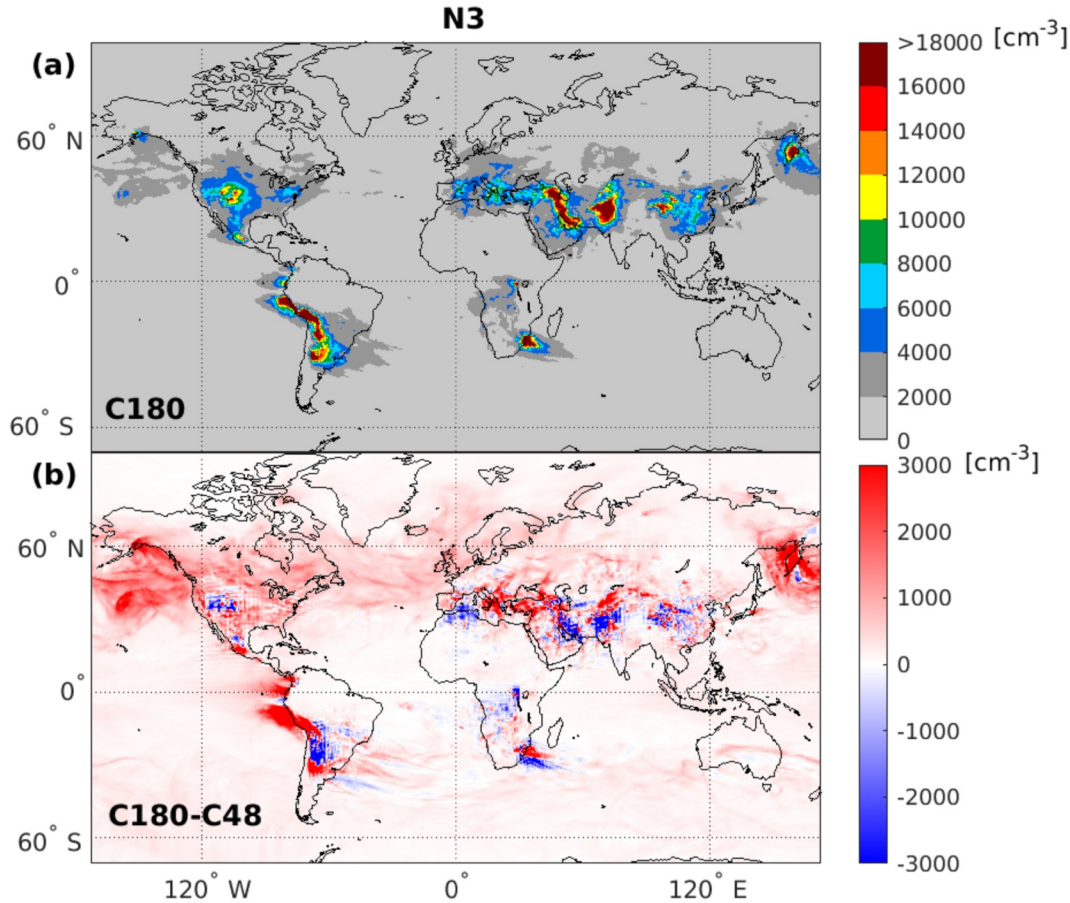

Figure 5. Geographic distribution of the simulated monthly mean (August 2019) (a) total particle number concentration (N3, particles with diameters larger than 3 nm) for the free-tropospheric layer at about 4 km for GCHP-TOMAS at C180 resolution (about 50 km × 50 km grid box size, globally), and (b) the N3 difference between C180 and C48 resolution (about 200 km × 200 km, globally) (C180–C48). Positive values indicate that C180 exceeds C48, and negative values indicate that C48 exceeds C180.

coarse- (C48) resolution model in the free troposphere at about 4 km altitude. The negative differences are mostly over the continents where C180 captures greater spatial heterogeneity than the C48 resolution. Total number concentrations are more strongly increased in the free troposphere at about 4 km altitude than for the surface layer (Figure S1 in Supporting Information S1). These increases in the free troposphere contribute to a 24.7% global mean increase in the N3 tropospheric column burden, which has a similar geographic distribution to Figure 5 (Figure S2 in Supporting Information S1). Considering the global mean size distribution in the free troposphere at about 4 km altitude, number increases at all simulated sizes but most toward the ultrafine sizes (Figure S3 in Supporting Information S1). Using preliminary results from our timing tests, the global mean number concentrations (at about 4 km altitude) exhibit monotonic increase with resolution that appears to be approaching an asymptote toward the finest resolutions (Figure S4 in Supporting Information S1).

Table 4 summarizes the global difference metrics for C180 to C48 for the free troposphere layer at about 4 km altitude. The global NMD for N3 is more strongly positive (+18.5%) than for the surface layer (Table 3), indicating a less even match between regions of positive and negative differences between C180 and C48 in the free troposphere versus near Earth's surface. The free-tropospheric NMD is also greater over-ocean versus over-land regions. The over-ocean NMDs are +23.3% for N3, +39.8% for sub-10 nm particles, and +13.1% for particles with diameters larger than 50 nm (N50). The sub-10 nm particles have the largest NMD across all size ranges. The NRMSDs are generally less or similar in the free-tropospheric layer (Table 4) relative to the surface layer (Table 3). These findings indicate that although the degree of spatial heterogeneity may be less in the free troposphere than at the surface (since mixing with transport can reduce spatial heterogeneity), the number

Table 4
C180 to C48 August 2019 Mean Free-Tropospheric (About 4 km Altitude) Particle Number Difference Metrics: Normalized Root Mean Square Difference (NRMSD) and Normalized Mean Difference (NMD) as Defined in Equations 1 and 2

	N3[a]	N50[b]	N_10_50[c]	N_sub10[d]
Global				
NRMSD[e] (%)	69.8	18.5	67.2	135.1
NMD[f] (%)	18.5	11.5	14.4	27.8
Ocean				
NRMSD (%)	65.8	19.9	66.4	140.0
NMD (%)	23.3	13.1	18.5	39.8
Land				
NRMSD (%)	64.6	16.0	63.7	108.9
NMD (%)	13.0	9.2	8.4	18.2

[a]Number of particles with diameters larger than 3 nm. [b]Number of particles with diameters larger than 50 nm. [c]Number of particles with diameters between 10 and 50 nm. [d]Number particles with diameters less than 10 nm. [e]Metrics are defined in the text of Section 3.2 and here refer to the model layer at about 4 km altitude considering global, over-land and over-ocean regions. [f]Positive NMD indicates that C180 has larger concentrations than C48 and negative NMD indicates that C48 has larger concentrations than C180.

concentrations are more strongly increased overall for fine (C180) versus coarse (C48) resolution in the free troposphere than at the surface. Contributors to these differences are examined further in the following section.

Vertical profiles of simulated global mean number concentrations for the C180 and C48 simulations are shown in Figure 6. For all particle size ranges, differences are relatively small within 2 km of the surface and are greater above 2 km. Thus, particle number concentrations in free troposphere show greater global-mean changes with model horizontal spatial resolution than near to Earth's surface. The N50 differences of about 15% in the free troposphere are expected to be climate relevant since these sizes affect aerosol optical depth and radiative effects. These free-tropospheric regions can be strongly controlled by secondary particle formation and growth processes since these regions are remote from most primary particle emission sources, which are Earth-surface based.

To further explore the mechanisms (Figure 1) contributing to these differences, we examined monthly (August 2019) and zonal mean vertical profiles of simulated aerosol mass concentrations and wet removal efficiency. For the fine- (C180) versus coarse- (C48) resolution simulation, zonal and August 2019 monthly mean sulfate and organic matter mass concentrations are reduced in the lowest 1–2 km of the troposphere and increased above 2 km (Figures S5 and S6 in Supporting Information S1), providing evidence that upward transport is enhanced toward finer model resolution. We found similar changes for other aerosol species (not shown). These resolution-dependent increases in aerosol mass loading in the free troposphere are consistent with previous studies using the GEOS-Chem model (K. Yu et al., 2018). We also found evidence that convective wet removal became less efficient toward finer resolution (Figure S7 in Supporting Information S1),

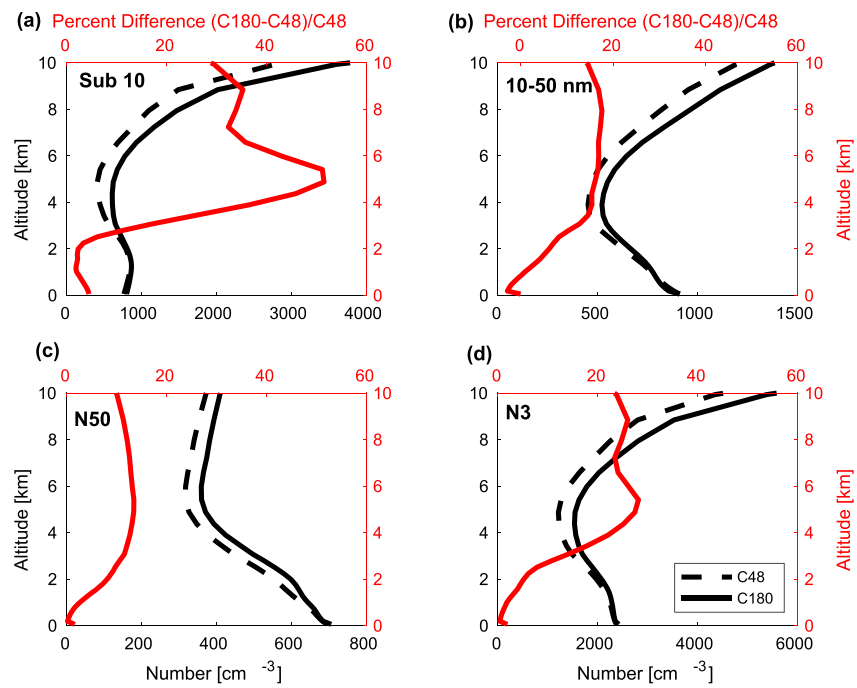

Figure 6. Vertical profiles of simulated global monthly mean (August 2019) number concentrations at C48 and C180 global resolution and their percent difference for particle size ranges of (a) Sub 10: number of particles with diameters less than 10 nm; (b) 10–50 nm: number of particles with diameters of 10–50 nm; (c) N50 number of particles with diameters larger than 50 nm; and (d) N3: total particle number (including all particles with diameters larger than 3 nm). Red and black axes refer to the red and black line plots, respectively.

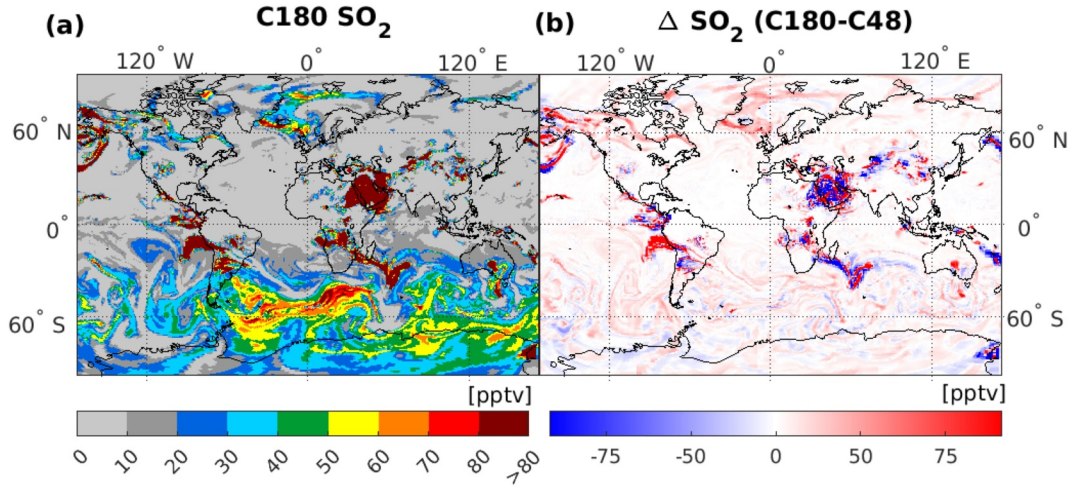

Figure 7. Global geographic distribution of (a) simulated free-tropospheric SO_2 mixing ratios at an altitude of about 4 km for GCHP-TOMAS at C180 resolution (about 50 km × 50 km grid box size, globally) and (b) the difference between C180 and C48 (about 200 km × 200 km grid box size, globally), for 1 September 2019 at 18 UTC. Positive differences indicate that C180 has greater mixing ratios than C48.

as also discussed by Williamson et al. (2019). Another study with a global model (NICAM.16) found similar effects between fine and coarse resolution (Goto et al., 2020). Complete re-mixing of cloudy and clear fractions at each model time step across progressively smaller grid boxes toward finer resolution contributes to this effect. Separate in-cloud aerosol tracers would help to address the excessive clear-cloudy mixing at coarse resolution in GEOS-Chem. The preceding factors enable stronger injection of particles and their precursors to higher altitudes toward fine resolution, which will lengthen their lifetimes as removal processes are less efficient toward higher altitudes (as shown by Croft et al. (2014) using the GEOS-Chem model and Figure S7 in Supporting Information S1). Thus, toward finer model resolution, enhanced upward transport, reduced convective removal efficiency, and longer lifetimes with higher altitude injection are expected to enhance particle precursors in the free troposphere (Figure 1). The impact of these factors on particle number has not been previously explored with the GEOS-Chem model and is examined further in the following section.

3.4. Resolution Dependence of Particle Precursors, Ultrafine Particles, and Aerosol Microphysical Rates

SO_2 is a key particle precursor. An example of the geographic distribution of free-tropospheric SO_2 plumes simulated by the GCHP-TOMAS model for 1 September 2019 at 18 UTC is shown in Figure 7. This example is typical of other hourly snapshots throughout the troposphere that can be taken from GCHP-TOMAS simulations. Figure 7 shows that the finer resolution simulation (C180) has several plumes with higher mixing ratios relative to the coarser resolution simulation (C48). These stronger plumes at C180 than C48 are particularly evident over boreal North America, the North Atlantic Ocean, and over the Pacific Ocean to the west of South America, at this example time. Several of these more concentrated plumes at fine versus coarse resolution maintain their stronger identity over distances in the order of 1,000s of km. This finding agrees with previous studies with GCHP's dynamical core revealing that as a result of numerical diffusion; coarsening spatial resolution typically led to more dilute chemical plumes and, hence, often have lower concentrations than observed values (Zhuang et al., 2018). As well, for the time of this case study, the global mean SO_2 mixing ratios at about 4 km altitude for the C180 resolution exceeded C48 by 32.6%. This increased free-tropospheric SO_2 loading toward finer resolution is evidence of an enhancement of upward transport with resolution. Further evidence of enhanced upward transport toward finer resolution is provided by the zonal and monthly mean vertical profiles of SO_2 mixing ratios, which for fine versus coarse resolution show mostly positive differences above about 2 km altitude versus below 2 km (Figure S8 in Supporting Information S1), similar to our finding for aerosol mass concentrations. We also examined the monthly SO_2 column burdens and found an 8.9% global mean enhancement (Figure S9 in Supporting Information S1) for the C180 relative to C48 resolution, indicating longer SO_2 lifetimes (due to more presence in the free troposphere) since related global total emissions are identical between resolutions.

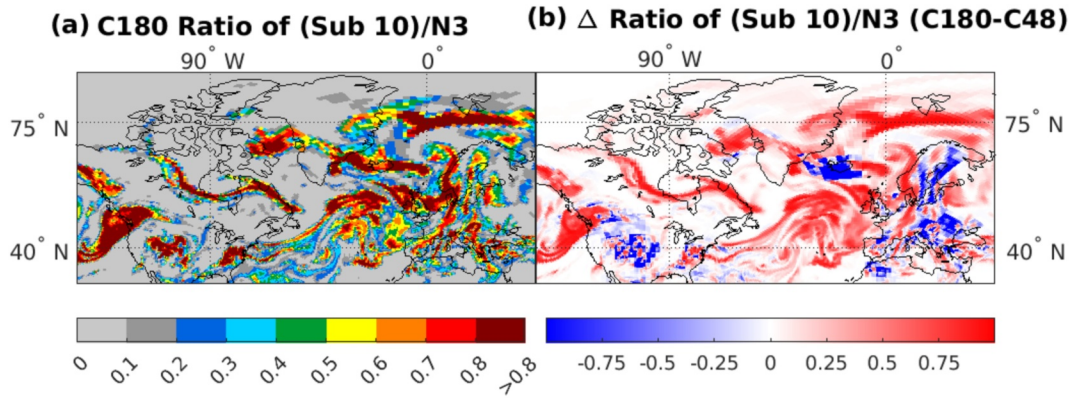

Figure 8. Geographic distribution of simulated (a) free-tropospheric fractional contribution of sub-10 nm particles to total number of particles at an altitude of about 4 km for GCHP-TOMAS at C180 resolution (about 50 km × 50 km grid box size, globally) and (b) the difference in this number ratio between C180 and C48 (C180–C48) for 1 September 2019 at 18 UTC considering a zoomed-in view over the Northern Hemisphere.

Since SO_2 is a key precursor for new particle formation in our simulations, these higher concentrations of particle precursors in the free troposphere can facilitate higher rates of new particle formation. Zonal and monthly mean vertical profiles of the simulated rate of nucleation of new particles show strengthening new particle formation (NPF) toward finer resolution in GCHP-TOMAS through much of the free troposphere, particularly in the summertime hemisphere (Figure S10 in Supporting Information S1).

We now consider 1 September 2019 at 18 UTC as a case study to demonstrate these resolution related changes. Figure 8a highlights regions of new particle formation at the time of this case study by showing the geographic distribution of the ratio of the number of sub-10 nm particles to total particle number for the fine (C180) resolution simulation in the free troposphere (about 4 km altitude) with a zoomed-on view over the Northern Hemisphere. Figure 8b shows the difference in this ratio between our two simulations (C180–C48). There are enhancements in this ratio over boreal North America and the North Atlantic Ocean near the locations of the SO_2 plumes (Figure 7), evidence of enhancement of plume concentrations toward finer resolution (Figure 1).

Next, we examine the North American continental outflow region over the western North Atlantic Ocean at 18 UTC on 1 September 2019 and explore how the cascade of resolution-dependent factors (Figure 1) impact particle number in the free troposphere. Figures 9 and 10 show plumes of particle precursors (SO_2, NH_3, and H_2O) and particle number concentrations, respectively, in the North American eastern coast continental outflow region for 1 September 2019 at 18 UTC and about 4 km altitude. The maximum particle precursor mixing ratios are more than 2-fold larger in the plumes at C180 relative to C48 (Figure 9). In a similar geographic pattern as the precursors, particle number concentrations are greater in the outflow plumes at C180 relative to C48 (Figure 10). Similar examples for boreal North America and western Peru are shown in Figures S11–S14 of the Supporting Information S1.

Figure 11 shows aerosol microphysical process (nucleation (also termed NPF) and number loss by coagulation) rates associated with the plumes in the east coast North American continental outflow region, for the same timeframe as Figures 9 and 10. Plumes of stronger nucleation rates are evident at C180 compared to C48. These processes are nonlinear; and as a result, even if we re-grid our two simulations to the same horizontal resolution, the particle formation rates remain greater at C180 versus C48 (as is illustrated by the differences shown in Table 4). The plumes of stronger nucleation rates are co-located greater precursor concentrations (Figure 9). Figure 11 shows a similar behavior for rates of number loss due to coagulation, which is another nonlinear microphysical process. There are plumes of stronger coagulation losses at C180 relative to C48. Greater variability in particle sizes favors stronger lowering of particle number by coagulation, as seen for C180 relative to C48. However, at this time of day there is a net gain in particle number in these regions at C180 versus C48 due to the more vigorous new particle formation. Similar examples are shown for boreal North America and western Peru in Figures S15 and S16 of the Supporting Information S1.

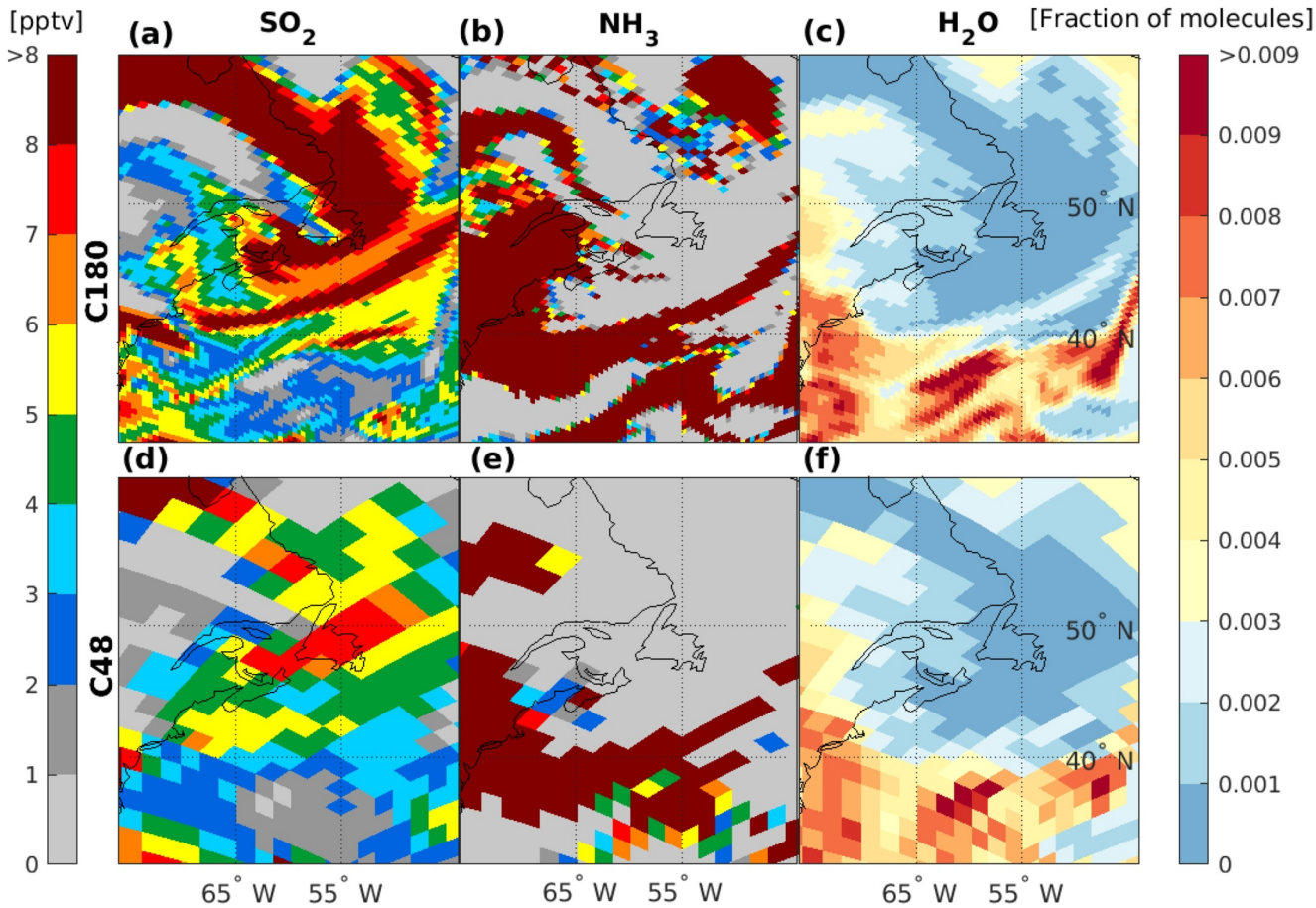

Figure 9. Geographic distribution of simulated free-tropospheric particle precursors at C180 resolution (about 50 km × 50 km grid box size, globally) for (a) SO_2, (b) NH_3, and (c) H_2O at an altitude of about 4 km over the east coast of North America for GCHP-TOMAS simulations for 1 September 2019 at 18 UTC and (d)–(f) similar at C48 resolution (about 200 km × 200 km grid box size, globally). Left color bar is for the 2 leftmost columns and right color bar is for the right-side column.

The cascade of factors leading to enhanced free-tropospheric particle precursors and NPF toward finer resolution (Figure 1) is also expected to influence the rates of condensation of condensable organic vapors and sulfuric acid in the free troposphere. Considering the zonal and monthly mean vertical profiles, we found stronger rates of both sulfuric acid and organic mass condensation in the free troposphere above about 2 km for the fine- (C180) versus coarse- (C48) resolution simulation (Figures S17 and S18, respectively in Supporting Information S1). We also examined the vertical profiles of global and monthly mean (August 2019) rates of change in number concentration due to sulfuric acid and organic vapor condensation (Figure S19, respectively in Supporting Information S1). Similar to the zonal profiles, global mean rates of number change due to sulfuric acid and organic vapor condensation have larger magnitudes at fine versus coarse resolution. Since condensation rates themselves are linear in nature, this magnitude enhancement at C180 relative to C48 resolution provides further evidence of stronger vertical transport into the free troposphere of particle precursors at fine versus coarse resolution. Differences in the shape of simulated organic and sulfuric acid condensation profiles arise in part because half of the SOA precursors are immediately available for condensation on emission unlike the sulfuric acid precursors.

In summary, a cascade of factors contributes to the dependency of aerosol number concentrations on global-model horizontal resolution (Figure 1). In GCHP-TOMAS, the net effect of these factors is a 11.5% increase in global and monthly mean tropospheric number column burden for particles with diameters larger than 50 nm (N50), which are of climate relevance. The N3 and N50 zonal and August 2019 monthly mean concentrations increase at all latitudes in the free troposphere above about 2 km (Figures S20 and S21 in Supporting Information S1). Enhancements occur across all particle sizes when comparing the global mean size distributions for fine- and coarse- model resolutions in the free troposphere at about 4 km altitude (Figure S3 in Supporting

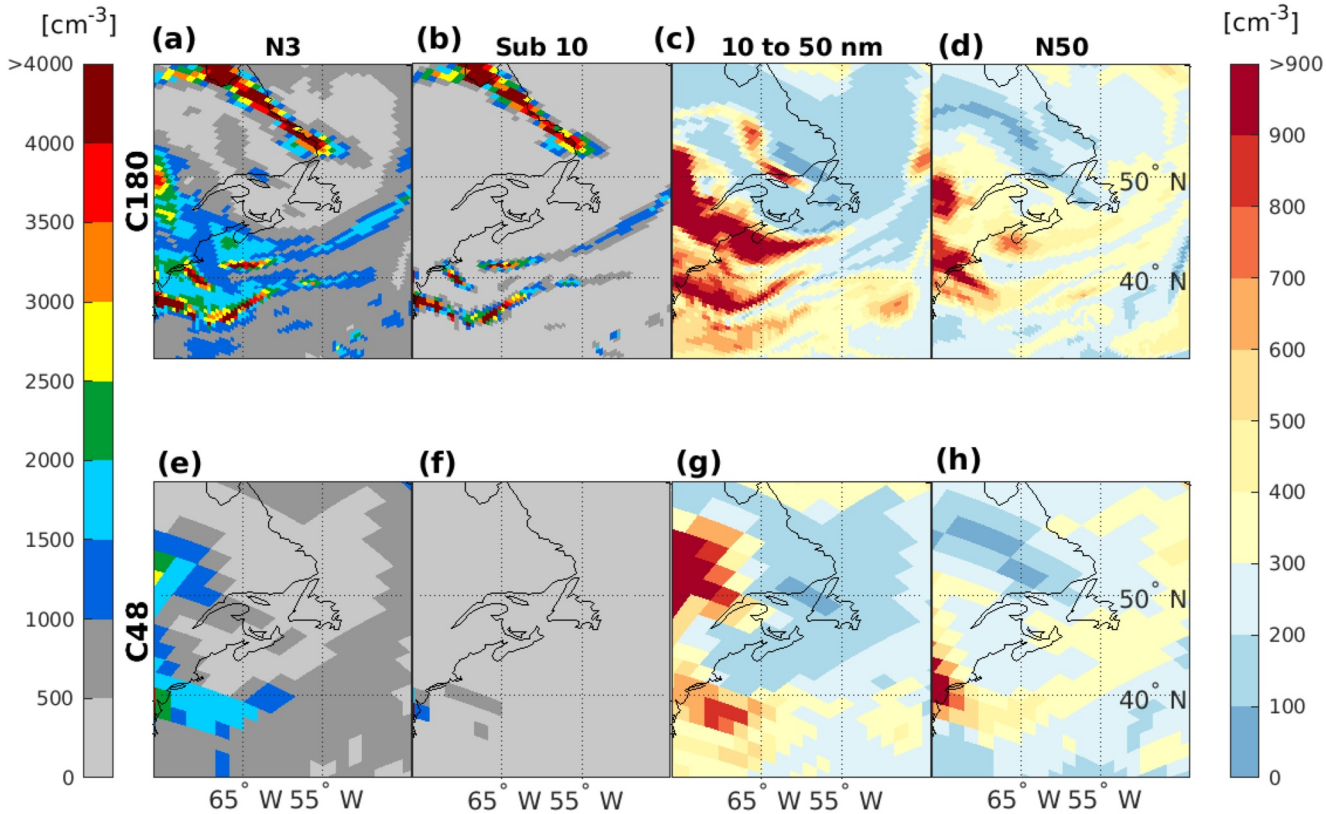

Figure 10. Geographic distribution of simulated free-tropospheric particle number concentrations for 4 size ranges at an altitude of about 4 km over the east coast of North America for GCHP-TOMAS simulations for 1 September 2019 at 18 UTC at C180 resolution (about 50 km × 50 km grid box size, globally) for (a) N3: all particles larger than 3 nm in diameter; (b) Sub 10: particles with diameters smaller than 10 nm; (c) 10–50 nm: particles with diameters in the range of 10–50 nm; (d) N50: particles with diameters larger than 50 nm and (e)–(h) similar at C48 resolution (about 200 km × 200 km grid box size, globally). Left color bar for the 2 leftmost columns and right color bar is for the 2 rightmost columns.

Information S1). These number enhancements toward fine model resolution are strongest in remote regions (i.e., in the free troposphere and particularly over the oceans, Tables 3 and 4). On the other hand, for the near-surface layer, the global and monthly mean number concentration change with resolution is close to zero. The set of factors examined in the preceding sections help to understand this near-zero change. Near the surface, aerosol mass loading decreases due to more vigorous upwards transport toward finer resolution (Figures S5 and S6 in Supporting Information S1). This effect promotes particle formation since condensable vapors are more likely to form new particles than condense on existing aerosols. In opposition, there is a simultaneous loss of particle precursors near the surface, due to the enhanced upward transport toward finer resolution. This opposing effect suppresses particle formation and growth such that the global mean number change is nearly zero in the surface layer. Our findings suggest that a fine and consistent global resolution is of importance for global-scale studies and for simulations considering the impacts of intercontinental transport over distances of 1,000s of km since regionally fine resolution (nested) simulations cannot capture the above noted effects.

4. Conclusions

The resolution dependence of nonlinear processes in global models has motivated work to increase spatial resolution. In particular, the highly nonlinear nature of size-resolved aerosol microphysical processes, their nonlinear interactions with dynamics and chemistry, and their reliance on resolution-dependent particle-precursor plume strength are well-suited to benefit from increased global model spatial resolution. However, the high computational demands of representing size-resolved particle formation and growth processes have previously been a limiting factor on increasing spatial resolution of aerosol microphysics simulations in global models. In this study, we employed the TwO-Moment Aerosol Sectional (TOMAS) scheme, which had been limited to a global spatial resolution of 2° × 2.5° and could only run on a single computing node in the classic configuration (GCC) of the

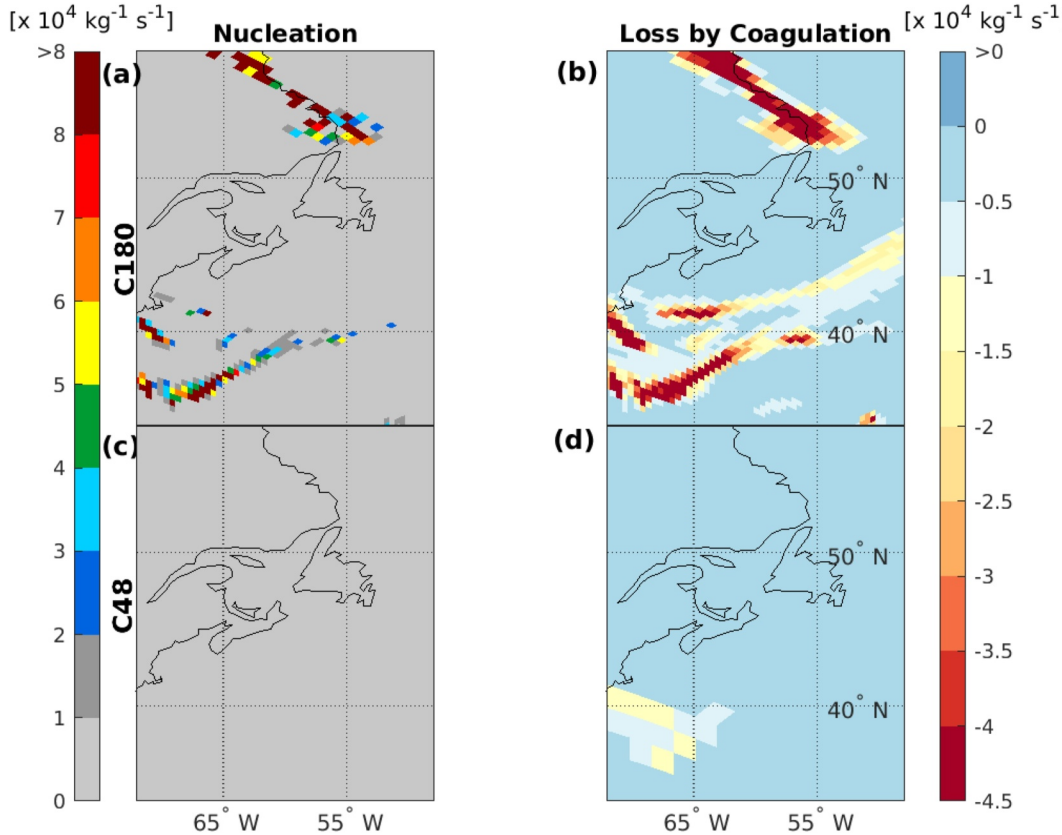

Figure 11. Geographic distribution of C180-resolution (about 50 km × 50 km grid box size, globally) simulated free-tropospheric rates of (a) nucleation (new particle formation, NPF) and (b) number loss by coagulation at an altitude of about 4 km over the east coast of North America for GCHP-TOMAS simulations for 1 September 2019 at 18 UTC and (c), (d) similar for C48 resolution (about 200 km × 200 km grid box size, globally). Left color bar is for the leftmost column and right color bar is for the rightmost column.

GEOS-Chem chemical transport model. Here, we took advantage of the distributed memory capability offered by the High-Performance configuration of GEOS-Chem (GCHP) (Eastham et al., 2018; Martin et al., 2022) and made the first implementation of TOMAS microphysics (Adams & Seinfeld, 2002; Kodros & Pierce, 2017) in GCHP (GCHP-TOMAS). This novel coupling of TOMAS with GCHP enabled examination of faster global simulations with finer global resolution (up to 25 km × 25 km, about 50-fold more grid boxes) than had been previously possible with TOMAS microphysics. As part of this effort, we developed the capability for GCHP-TOMAS simulations on the AWS cloud to increase accessibility of its use. Below we focus on model performance and the impact of changes in horizontal resolution on simulations of aerosol number and size.

Based on our timing performance tests, the GCHP-TOMAS model exhibited near ideal scalability between number of computing cores employed and computing time, when using horizontal resolutions ranging from about 25 km × 25 km (termed C360) to about 400 km × 400 km (termed C24). The fastest GCHP-TOMAS runtime (also referred to as wall time) for our finest global resolution (C360) GCHP-TOMAS simulation was about 43 hr of real time to simulate 7 days with the use of 960 physical cores (30 nodes). Our results showed that a user with 360 physical cores available could achieve GCHP-TOMAS 7-day simulation wall times of about 16 hr for C180 (about 50 km × 50 km global resolution) and 3 hr for C90 (about 100 km × 100 km global resolution). These wall times are about double the wall times for the GCHP model without the TOMAS microphysics (Martin et al., 2022), similar to the GCC-TOMAS to GCC wall time ratio.

We compared fine (termed, C180) and coarse (termed, C48) horizontal resolution monthly mean (August 2019) simulations of aerosol number and size with GCHP-TOMAS and found that simulated global mean aerosol number concentrations increased with model resolution. These increases were strongest over ocean regions, in the free troposphere, and for ultra-fine particles (with diameters less than 50 nm). In the model's surface layer, greater

spatial heterogeneity of particle number was represented by the C180 relative to the C48 simulation, demonstrated by global normalized root mean square differences (NRMSD) of 92.1% for total particle number. However, for the model's surface layer, the global mean increase in total particle number was only +2% (i.e., C180 larger relative to C48) due to cancellation of areas with positive and negative differences between the two resolutions. On the other hand, in the free troposphere at about 4 km altitude, the change in global mean total particle number (all sizes larger than 3 nm) was +18.5% (i.e., C180 larger relative to C48), and over the oceans was +23.3% (total over all sizes), +39.8% (sub-10 nm diameter sizes) and +13.1% (diameters larger than 50 nm). Conversely, the free-tropospheric layer NRMSD was less (69.8%) relative to the surface layer, indicating less spatial heterogeneity between the two simulations in the free troposphere than toward the surface. We found a 11.5% increase in global mean tropospheric number column burden for particles with diameters larger than 50 nm (N50), which are of climate relevance.

A cascade of factors (Figure 1) contributed to these enhancements in size-resolved number concentrations. Previous studies using the GEOS-Chem model and its dynamical core found that upwards transport increases with model horizontal resolution (K. Yu et al., 2018) combined with weaker convective wet removal (Williamson et al., 2019) and longer lifetimes of precursors and particles with higher altitude injections (Croft et al., 2014). In our simulations, these factors led to enhanced free tropospheric particle precursors concentrations, which occurred in more concentrated plumes. Decreasing numerical diffusion with increasing resolution also contributed to the plume structure (Eastham & Jacob, 2017; Zhuang et al., 2018). An examination of hourly mean output from our simulations revealed that free-tropospheric plumes of particle precursors (SO_2, NH_3, and H_2O) can retain higher concentrations over distances in the order of 1,000s of km from emission point at finer (C180) relative to coarser (C48) resolution. These enhancements in precursor mixing ratios promoted areas of stronger rates of new particle formation and growth in the fine versus coarse resolution simulation in the free troposphere, despite stronger rates of coagulation. Thus, particle-precursor concentrations changes combined with the nonlinearity of particle formation/growth processes, as well as vertical transport and removal differences all contributed to the enhancements in monthly mean number concentrations (particularly among the smallest particle sizes in the free troposphere) for the fine relative to coarse simulation with GCHP-TOMAS. Near the Earth surface in the model, a balance between lower condensation sink (promoting new particle formation) and a loss of particle precursors (suppressing new particle formation and growth) yielded little change in global mean number concentrations with horizontal resolution.

In summary, finer resolution global models are desirable for their capability to capture magnitudes and spatial heterogeneity of size-resolved aerosol number concentrations relative to coarser resolution models. Our findings highlight that horizontal spatial resolution has a strong impact on size-resolved aerosol microphysics simulations with the potential to alter understanding based upon coarse resolution simulations. These results suggest that a fine and consistent global resolution is of importance for global-scale studies and simulations considering long-range/intercontinental transport. Future work is needed to compare with other global and regional models with fine-resolution aerosol-microphysics capability for a more extensive characterization of the magnitude of the resolution dependency of particle number and size. Detailed model-measurement comparisons are also needed as part of this future work, along with additional work to examine the impact of vertical resolution on size-resolved aerosol microphysics simulations. Further work is also needed to examine the variation of microphysical processes rates with horizontal resolution and to identify if process parameterizations that have been designed for a certain range of coarser global model resolutions need to be modified for implementation in finer resolution global models. In addition, future work should extend the resolution-independent capability for dust emissions (Meng et al., 2021, 2022) to GCHP-TOMAS. Lastly, extension of this investigation to other months and assessing the broader impacts on simulated global aerosol effective radius, optical depth and radiative forcing are also warranted. Addressing these knowledge gaps will help to reduce uncertainty in simulations of both air quality and climate effects of aerosols and their spatial heterogeneity.

Data Availability Statement

Modifications to implement TOMAS aerosol microphysics in GCHP are available at https://doi.org/10.5281/zenodo.10026771 (The International GEOS-Chem User Community, 2023a), https://doi.org/10.5281/zenodo.10026853 (The International GEOS-Chem User Community, 2023b), and https://doi.org/10.5281/zenodo.10026844 (The International GEOS-Chem User Community, 2023c). The GCHP release versions used in this

study are available at https://doi.org/10.5281/zenodo.5764877 for version 13.3.4 (The International GEOS-Chem User Community, 2021) and https://doi.org/10.5281/zenodo.8411829 for version 14.2.0 (The International GEOS-Chem User Community, 2023d). The updates to implement TOMAS are also available in the release version of GCHP (version 14.3.0) at https://doi.org/10.5281/zenodo.10640559 (The International GEOS-Chem User Community, 2024).

Acknowledgments
The authors thank the three anonymous reviewers for their invaluable contributions to the review process. BC and RY-WC thank Balagopal Pillai for maintaining and updating the computing platform at Dalhousie University. The authors are grateful for funding from the Ocean Frontier Institute through an award from the Canada First Research Excellence Fund. Work at Washington University was supported by NASA Grant 80NSSC20K0281 and by the NSF Grant 2244984 while work at Colorado State University was supported by NASA Grant 80NSSC21K0429 and by the NSF Grant 1950327.

References

Adams, P. J., & Seinfeld, J. H. (2002). Predicting global aerosol size distributions in general circulation models. *Journal of Geophysical Research*, *107*(19), 1–23. https://doi.org/10.1029/2001JD001010

Albrecht, B. A. (1989). Aerosols, cloud microphysics, and fractional cloudiness. *Science*, *245*(4923), 1227–1230. https://doi.org/10.1126/science.245.4923.1227

Almeida, J., Schobesberger, S., Kürten, A., Ortega, I. K., Kupiainen-Määttä, O., Praplan, A. P., et al. (2013). Molecular understanding of sulphuric acid-amine particle nucleation in the atmosphere. *Nature*, *502*(7471), 359–363. https://doi.org/10.1038/nature12663

Amos, H. M., Jacob, D. J., Holmes, C. D., Fisher, J. A., Wang, Q., Yantosca, R. M., et al. (2012). Gas-particle partitioning of atmospheric Hg(II) and its effect on global mercury deposition. *Atmospheric Chemistry and Physics*, *12*(1), 591–603. https://doi.org/10.5194/acp-12-591-2012

Bellouin, N., Quaas, J., Gryspeerdt, E., Kinne, S., Stier, P., Watson-Parris, D., et al. (2020). Bounding global aerosol radiative forcing of climate change. *Reviews of Geophysics*, *58*(1), e2019RG000660. https://doi.org/10.1029/2019RG000660

Bey, I., Jacob, D. J., Yantosca, R. M., Logan, J. A., Field, B. D., Fiore, A. M., et al. (2001). Global modeling of tropospheric chemistry with assimilated meteorology: Model description and evaluation. *Journal of Geophysical Research*, *106*(D19), 23073–23095. https://doi.org/10.1029/2001JD000807

Bindle, L., Martin, R. V., Cooper, M. J., Lundgren, E. W., Eastham, S. D., Auer, B. M., et al. (2021). Grid-stretching capability for the GEOS-Chem 13.0.0 atmospheric chemistry model. *Geoscientific Model Development*, *14*(10), 5977–5997. https://doi.org/10.5194/gmd-14-5977-2021

Cai, R., Häkkinen, E., Yan, C., Jiang, J., Kulmala, M., & Kangasluoma, J. (2022). The effectiveness of the coagulation sink of 3–10 nm atmospheric particles. *Atmospheric Chemistry and Physics*, *22*(17), 11529–11541. https://doi.org/10.5194/acp-22-11529-2022

Charlson, R. J., Lovelock, J. E., Andreae, M. O., & Warren, S. G. (1987). Oceanic phytoplankton, atmospheric sulphur, cloud albedo and climate. *Nature*, *326*(6114), 655–661. https://doi.org/10.1038/326655a0

Cohen, A. J., Brauer, M., Burnett, R., Anderson, H. R., Frostad, J., Estep, K., et al. (2017). Estimates and 25-year trends of the global burden of disease attributable to ambient air pollution: An analysis of data from the Global Burden of Diseases Study 2015. *The Lancet*, *389*(10082), 1907–1918. https://doi.org/10.1016/S0140-6736(17)30505-6

Croft, B., Pierce, J. R., & Martin, R. V. (2014). Interpreting aerosol lifetimes using the GEOS-Chem model and constraints from radionuclide measurements. *Atmospheric Chemistry and Physics*, *14*(8), 4313–4325. https://doi.org/10.5194/acp-14-4313-2014

Dinkelacker, B. T., Rivera, P. G., Kioutsioukis, I., Adams, P. J., & Pandis, S. N. (2022). Evaluation of high-resolution predictions of fine particulate matter and its composition in an urban area using PMCAMx-v2.0. *Geoscientific Model Development*, *15*(23), 8899–8912. https://doi.org/10.5194/gmd-15-8899-2022

Dunne, E. M., Gordon, H., Kurten, A., Almeida, J., Duplissy, J., Williamson, C., et al. (2016). Global atmospheric particle formation from CERN CLOUD measurements. *Science*, *354*(6316), 1119–1124. https://doi.org/10.1126/science.aaf2649

Earth System Modeling. (2023). Regridding. Retrieved from https://earthsystemmodeling.org/regrid/

Eastham, S. D., & Jacob, D. J. (2017). Limits on the ability of global Eulerian models to resolve intercontinental transport of chemical plumes. *Atmospheric Chemistry and Physics*, *17*(4), 2543–2553. https://doi.org/10.5194/acp-17-2543-2017

Eastham, S. D., Long, M. S., Keller, C. A., Lundgren, E., Yantosca, R. M., Zhuang, J., et al. (2018). GEOS-Chem High Performance (GCHP v11-02c): A next-generation implementation of the GEOS-Chem chemical transport model for massively parallel applications. *Geoscientific Model Development*, *11*(7), 2941–2953. https://doi.org/10.5194/gmd-11-2941-2018

Emerson, E. W., Hodshire, A. L., Debolt, H. M., Bilsback, K. R., Pierce, J. R., McMeeking, G. R., & Farmer, D. K. (2020). Revisiting particle dry deposition and its role in radiative effect estimates. *Proceedings of the National Academy of Sciences*, *117*(42), 26076–26082. https://doi.org/10.1073/pnas.2014761117

Feng, X., Lin, H., Fu, T.-M., Sulprizio, M. P., Zhuang, J., Jacob, D. J., et al. (2021). WRF-GC (v2.0): Online two-way coupling of WRF (v3.9.1.1) and GEOS-Chem (v12.7.2) for modeling regional atmospheric chemistry–meteorology interactions. *Geoscientific Model Development*, *14*(6), 3741–3768. https://doi.org/10.5194/gmd-14-3741-2021

Fuchs, N. A. (1964). In C. N. Davies (Ed.), *The mechanics of aerosols. By N. A. Fuchs. Translated by R. E. Daisley and Marina Fuchs* (Vol. 91, No. (388), p. 249). (Pergamon Press), Quarterly Journal of the Royal Meteorological Society. Xiv, 408; 82 Figures; 40 Tables. £6. https://doi.org/10.1002/qj.49709138822

Gelaro, R., McCarty, W., Suárez, M. J., Todling, R., Molod, A., Takacs, L., et al. (2017). The modern-era retrospective analysis for research and applications, version 2 (MERRA-2). *Journal of Climate*, *30*(14), 5419–5454. https://doi.org/10.1175/JCLI-D-16-0758.1

GEOS-Chem. (2024). GEOS-Chem. Retrieved from https://geoschem.github.io/

Goto, D., Sato, Y., Yashiro, H., Suzuki, K., Oikawa, E., Kudo, R., et al. (2020). Global aerosol simulations using NICAM.16 on a 14 km grid spacing for a climate study: Improved and remaining issues relative to a lower-resolution model. *Geoscientific Model Development*, *13*(8), 3731–3768. https://doi.org/10.5194/gmd-13-3731-2020

Hill, C., DeLuca, C., Balaji, Suarez, M., & Da Silva, A. (2004). The architecture of the Earth system modeling framework. *Computing in Science & Engineering*, *6*(1), 18–28. https://doi.org/10.1109/MCISE.2004.1255817

Hoesly, R. M., Smith, S. J., Feng, L., Klimont, Z., Janssens-maenhout, G., Dawidowski, L., et al. (2018). Historical (1750–2014) anthropogenic emissions of reactive gases and aerosols from the Community Emissions Data System (CEDS). *Geoscientific Model Development*, *11*(1), 369–408. https://doi.org/10.5194/gmd-11-369-2018

Hu, L., Keller, C. A., Long, M. S., Sherwen, T., Auer, B., Da Silva, A., et al. (2018). Global simulation of tropospheric chemistry at 12.5 km resolution: Performance and evaluation of the GEOS-Chem chemical module (v10-1) within the NASA GEOS Earth system model (GEOS-5 ESM). *Geoscientific Model Development*, *11*(11), 4603–4620. https://doi.org/10.5194/gmd-11-4603-2018

Intergovernmental Panel on Climate Change (IPCC). (2023). *Climate change 2021–The physical science basis: Working group I contribution to the sixth assessment report of the intergovernmental panel on climate change*. Cambridge University Press. https://doi.org/10.1017/9781009157896

Jaeglé, L., Quinn, P. K., Bates, T. S., Alexander, B., & Lin, J.-T. (2011). Global distribution of sea salt aerosols: New constraints from in situ and remote sensing observations. *Atmospheric Chemistry and Physics*, *11*(7), 3137–3157. https://doi.org/10.5194/acp-11-3137-2011

Jin, X., Fiore, A. M., Curci, G., Lyapustin, A., Civerolo, K., Ku, M., et al. (2019). Assessing uncertainties of a geophysical approach to estimate surface fine particulate matter distributions from satellite-observed aerosol optical depth. *Atmospheric Chemistry and Physics*, *19*(1), 295–313. https://doi.org/10.5194/acp-19-295-2019

Keller, C. A., Knowland, K. E., Duncan, B. N., Liu, J., Anderson, D. C., Das, S., et al. (2021). Description of the NASA GEOS composition forecast modeling system GEOS-CF v1.0. *Journal of Advances in Modeling Earth Systems*, *13*(4). https://doi.org/10.1029/2020MS002413

Kerminen, V. M., Anttila, T., Lehtinen, K. E. J., & Kulmala, M. (2004). Parameterization for atmospheric new-particle formation: Application to a system involving sulfuric acid and condensable water-soluble organic vapors. *Aerosol Science and Technology*, *38*(10), 1001–1008. https://doi.org/10.1080/027868290519085

Kerminen, V.-M., Chen, X., Vakkari, V., Petäjä, T., Kulmala, M., & Bianchi, F. (2018). Atmospheric new particle formation and growth: Review of field observations. *Environmental Research Letters*, *13*(10), 103003. https://doi.org/10.1088/1748-9326/aadf3c

Kirkby, J., Curtius, J., Almeida, J., Dunne, E., Duplissy, J., Ehrhart, S., et al. (2011). Role of sulphuric acid, ammonia and galactic cosmic rays in atmospheric aerosol nucleation. *Nature*, *476*(7361), 429–435. https://doi.org/10.1038/nature10343

Kodros, J. K., & Pierce, J. R. (2017). Important global and regional differences in aerosol cloud-albedo effect estimates between simulations with and without prognostic aerosol microphysics. *Journal of Geophysical Research: Atmospheres*, *122*(7), 4003–4018. https://doi.org/10.1002/2016JD025886

Lee, S. S., Li, Z., Zhang, Y., Yoo, H., Kim, S., Kim, B.-G., et al. (2018). Effects of model resolution and parameterizations on the simulations of clouds, precipitation, and their interactions with aerosols. *Atmospheric Chemistry and Physics*, *18*(1), 13–29. https://doi.org/10.5194/acp-18-13-2018

Lee, Y. H., & Adams, P. J. (2012). A fast and efficient version of the TwO-Moment Aerosol Sectional (TOMAS) global aerosol microphysics model. *Aerosol Science and Technology*, *46*(6), 678–689. https://doi.org/10.1080/02786826.2011.643259

Lee, Y. H., Pierce, J. R., & Adams, P. J. (2013). Representation of nucleation mode microphysics in a global aerosol model with sectional microphysics. *Geoscientific Model Development*, *6*(4), 1221–1232. https://doi.org/10.5194/gmd-6-1221-2013

Li, C., Martin, R. V., Cohen, R. C., Bindle, L., Zhang, D., Chatterjee, D., et al. (2023). Variable effects of spatial resolution on modeling of nitrogen oxides. *Atmospheric Chemistry and Physics*, *23*(5), 3031–3049. https://doi.org/10.5194/acp-23-3031-2023

Li, J., Min, Q., Peng, Y., Sun, Z., & Zhao, J.-Q. (2015). Accounting for dust aerosol size distribution in radiative transfer: Dust size distribution for radiation. *Journal of Geophysical Research: Atmospheres*, *120*(13), 6537–6550. https://doi.org/10.1002/2015JD023078

Li, K., Jacob, D. J., Liao, H., Qiu, Y., Shen, L., Zhai, S., et al. (2021). Ozone pollution in the North China Plain spreading into the late-winter haze season. *Proceedings of the National Academy of Sciences of the United States of America*, *118*(10), e2015797118. https://doi.org/10.1073/pnas.2015797118

Lin, H., Feng, X., Fu, T.-M., Tian, H., Ma, Y., Zhang, L., et al. (2020). WRF-GC (v1.0): Online coupling of WRF (v3.9.1.1) and GEOS-Chem (v12.2.1) for regional atmospheric chemistry modeling—Part 1: Description of the one-way model. *Geoscientific Model Development*, *13*(7), 3241–3265. https://doi.org/10.5194/gmd-13-3241-2020

Lin, H., Jacob, D. J., Lundgren, E. W., Sulprizio, M. P., Keller, C. A., Fritz, T. M., et al. (2021). Harmonized Emissions Component (HEMCO) 3.0 as a versatile emissions component for atmospheric models: Application in the GEOS-Chem, NASA GEOS, WRF-GC, CESM2, NOAA GEFS-Aerosol, and NOAA UFS models. *Geoscientific Model Development*, *14*(9), 5487–5506. https://doi.org/10.5194/gmd-14-5487-2021

Liu, H., Jacob, D. J., Bey, I., & Yantosca, R. M. (2001). Constraints from ^{210}Pb and ^{7}Be on wet deposition and transport in a global three-dimensional chemical tracer model driven by assimilated meteorological fields. *Journal of Geophysical Research*, *106*(D11), 12109–12128. https://doi.org/10.1029/2000JD900839

Long, M. S., Keene, W. C., Easter, R. C., Sander, R., Liu, X., Kerkweg, A., & Erickson, D. (2014). Sensitivity of tropospheric chemical composition to halogen-radical chemistry using a fully coupled size-resolved multiphase chemistry–global climate system: Halogen distributions, aerosol composition, and sensitivity of climate-relevant gases. *Atmospheric Chemistry and Physics*, *14*(7), 3397–3425. https://doi.org/10.5194/acp-14-3397-2014

Long, M. S., Yantosca, R., Nielsen, J. E., Keller, C. A., da Silva, A., Sulprizio, M. P., et al. (2015). Development of a grid-independent GEOS-Chem chemical transport model (v9-02) as an atmospheric chemistry module for Earth system models. *Geoscientific Model Development*, *8*(3), 595–602. https://doi.org/10.5194/gmd-8-595-2015

Lu, X., Zhang, L., Wu, T., Long, M. S., Wang, J., Jacob, D. J., et al. (2020). Development of the global atmospheric chemistry general circulation model BCC-GEOS-Chem v1.0: Model description and evaluation. *Geoscientific Model Development*, *13*(9), 3817–3838. https://doi.org/10.5194/gmd-13-3817-2020

Mann, G. W., Carslaw, K. S., Reddington, C. L., Pringle, K. J., Schulz, M., Asmi, A., et al. (2014). Intercomparison and evaluation of global aerosol microphysical properties among AeroCom models of a range of complexity. *Atmospheric Chemistry and Physics*, *14*(9), 4679–4713. https://doi.org/10.5194/acp-14-4679-2014

Martin, R. V., Eastham, S. D., Bindle, L., Lundgren, E. W., Clune, T. L., Keller, C. A., et al. (2022). Improved advection, resolution, performance, and community access in the new generation (version 13) of the high-performance GEOS-Chem global atmospheric chemistry model (GCHP). *Geoscientific Model Development*, *15*(23), 8731–8748. https://doi.org/10.5194/gmd-15-8731-2022

Matsui, H. (2017). Development of a global aerosol model using a two-dimensional sectional method: 1. Model design: 2-D Sectional Global Aerosol Model 1. *Journal of Advances in Modeling Earth Systems*, *9*(4), 1921–1947. https://doi.org/10.1002/2017MS000936

Matsui, H., & Mahowald, N. (2017). Development of a global aerosol model using a two-dimensional sectional method: 2. Evaluation and sensitivity simulations: 2-D Sectional Global Aerosol Model 2. *Journal of Advances in Modeling Earth Systems*, *9*(4), 1887–1920. https://doi.org/10.1002/2017MS000937

McDuffie, E. E., Smith, S. J., O'Rourke, P., Tibrewal, K., Venkataraman, C., Marais, E. A., et al. (2020). A global anthropogenic emission inventory of atmospheric pollutants from sector- and fuel-specific sources (1970–2017): An application of the Community Emissions Data System (CEDS). *Earth System Science Data*, *12*(4), 3413–3442. https://doi.org/10.5194/essd-12-3413-2020

Meng, J., Huang, Y., Leung, D. M., Li, L., Adebiyi, A. A., Ryder, C. L., et al. (2022). Improved parameterization for the size distribution of emitted dust aerosols reduces model underestimation of super coarse dust. *Geophysical Research Letters*, *49*(8), e2021GL097287. https://doi.org/10.1029/2021GL097287

Meng, J., Martin, R. V., Ginoux, P., Hammer, M., Sulprizio, M. P., Ridley, D. A., & van Donkelaar, A. (2021). Grid-independent high resolution dust emissions (v1.0) for chemical transport models: Application to GEOS-Chem (version 12.5.0). *Geoscientific Model Development*, *14*(7), 4249–4260. https://doi.org/10.5194/gmd-14-4249-2021

Moorthi, S., & Suárez, M. J. (1992). Relaxed Arakawa-Schubert. A parameterization of moist convection for general circulation models. *Monthly Weather Review*, *120*(6), 978–1002. https://doi.org/10.1175/1520-0493(1992)120<0978:RASAPO>2.0.CO;2

Murray, L. T., Leibensperger, E. M., Orbe, C., Mickley, L. J., & Sulprizio, M. (2021). GCAP 2.0: A global 3-D chemical-transport model framework for past, present, and future climate scenarios. *Geoscientific Model Development*, *14*(9), 5789–5823. https://doi.org/10.5194/gmd-14-5789-2021

Myhre, G., Samset, B. H., Schulz, M., Balkanski, Y., Bauer, S., Berntsen, T. K., et al. (2013). Radiative forcing of the direct aerosol effect from AeroCom phase II simulations. *Atmospheric Chemistry and Physics*, *13*(4), 1853–1877. https://doi.org/10.5194/acp-13-1853-2013

Napari, I., Noppel, M., Vehkamäki, H., & Kulmala, M. (2002). Parametrization of ternary nucleation rates for H_2SO_4-NH_3-H_2O vapors. *Journal of Geophysical Research*, *107*(D19), 4381. https://doi.org/10.1029/2002JD002132

Pai, S. J., Heald, C. L., Pierce, J. R., Farina, S. C., Marais, E. A., Jimenez, J. L., et al. (2020). An evaluation of global organic aerosol schemes using airborne observations. *Atmospheric Chemistry and Physics*, *20*(5), 2637–2665. https://doi.org/10.5194/acp-20-2637-2020

Paolella, D. A., Tessum, C. W., Adams, P. J., Apte, J. S., Chambliss, S., Hill, J., et al. (2018). Effect of model spatial resolution on estimates of fine particulate matter exposure and exposure disparities in the United States. *Environmental Science and Technology Letters*, *5*(7), 436–441. https://doi.org/10.1021/acs.estlett.8b00279

Pierce, J. R., & Adams, P. J. (2009). A computationally efficient aerosol nucleation/condensation method: Pseudo-steady-state sulfuric acid. *Aerosol Science and Technology*, *43*(3), 216–226. https://doi.org/10.1080/02786820802587896

Pierce, J. R., Chen, K., & Adams, P. J. (2007). Contribution of primary carbonaceous aerosol to cloud condensation nuclei: Processes and uncertainties evaluated with a global aerosol microphysics model. *Atmospheric Chemistry and Physics*, *7*(20), 5447–5466. https://doi.org/10.5194/acp-7-5447-2007

Pierce, J. R., Croft, B., Kodros, J. K., D'Andrea, S. D., & Martin, R. V. (2015). The importance of interstitial particle scavenging by cloud droplets in shaping the remote aerosol size distribution and global aerosol-climate effects. *Atmospheric Chemistry and Physics*, *15*(11), 6147–6158. https://doi.org/10.5194/acp-15-6147-2015

Pierce, J. R., Riipinen, I., Kulmala, M., Ehn, M., Petäjä, T., Junninen, H., et al. (2011). Quantification of the volatility of secondary organic compounds in ultrafine particles during nucleation events. *Atmospheric Chemistry and Physics*, *11*(17), 9019–9036. https://doi.org/10.5194/acp-11-9019-2011

Pierce, J. R., Theodoritsi, G., Adams, P. J., & Pandis, S. N. (2009). Parameterization of the effect of sub-grid scale aerosol dynamics on aerosol number emission rates. *Journal of Aerosol Science*, *40*(5), 385–393. https://doi.org/10.1016/j.jaerosci.2008.11.009

Ramnarine, E., Kodros, J. K., Hodshire, A. L., Lonsdale, C. R., Alvarado, M. J., & Pierce, J. R. (2019). Effects of near-source coagulation of biomass burning aerosols on global predictions of aerosol size distributions and implications for aerosol radiative effects. *Atmospheric Chemistry and Physics*, *19*(9), 6561–6577. https://doi.org/10.5194/acp-19-6561-2019

Ramshaw, J. D. (1985). Conservative rezoning algorithm for generalized two-dimensional meshes. *Journal of Computational Physics*, *59*(2), 193–199. https://doi.org/10.1016/0021-9991(85)90141-X

Regayre, L. A., Johnson, J. S., Yoshioka, M., Pringle, K. J., Sexton, D. M. H., Booth, B. B. B., et al. (2018). Aerosol and physical atmosphere model parameters are both important sources of uncertainty in aerosol ERF. *Atmospheric Chemistry and Physics*, *18*(13), 9975–10006. https://doi.org/10.5194/acp-18-9975-2018

Riccobono, F., Schobesberger, S., Scott, C. E., Dommen, J., Ortega, I. K., Rondo, L., et al. (2014). Oxidation products of biogenic emissions contribute to nucleation of atmospheric particles. *Science*, *344*, 717–721. https://doi.org/10.1126/science.1243527

Riipinen, I., Pierce, J. R., Yli-Juuti, T., Nieminen, T., Häkkinen, S., Ehn, M., et al. (2011). Organic condensation: A vital link connecting aerosol formation to cloud condensation nuclei (CCN) concentrations. *Atmospheric Chemistry and Physics*, *11*(8), 3865–3878. https://doi.org/10.5194/acp-11-3865-2011

Sato, Y., Miura, H., Yashiro, H., Goto, D., Takemura, T., Tomita, H., & Nakajima, T. (2016). Unrealistically pristine air in the Arctic produced by current global scale models. *Scientific Reports*, *6*(1), 26561. https://doi.org/10.1038/srep26561

Suarez, M., Trayanov, A., Hill, C., Schopf, P., & Vikhliaev, Y. (2007). MAPL: A high-level programming paradigm to support more rapid and robust encoding of hierarchical trees of interacting high-performance components. In *Proceedings of the 2007 symposium on component and framework technology in high-performance and scientific computing* (pp. 11–20). https://doi.org/10.1145/1297385.1297388

Tegen, I., Neubauer, D., Ferrachat, S., Siegenthaler-Le Drian, C., Bey, I., Schutgens, N., et al. (2019). The global aerosol–climate model ECHAM6.3–HAM2.3—Part 1: Aerosol evaluation. *Geoscientific Model Development*, *12*(4), 1643–1677. https://doi.org/10.5194/gmd-12-1643-2019

The International GEOS-Chem User Community. (2021). geoschem/GCHP: GCHP 13.3.4 (13.3.4) [Software]. *Zenodo*. https://doi.org/10.5281/zenodo.5764877

The International GEOS-Chem User Community. (2023a). BettyCroft/GCHP: GCHP-TOMAS (13.3.4) [Software]. *Zenodo*. https://doi.org/10.5281/zenodo.10026771

The International GEOS-Chem User Community. (2023b). BettyCroft/geos-chem (13.3.4.test5) [Software]. *Zenodo*. https://doi.org/10.5281/zenodo.10026853

The International GEOS-Chem User Community. (2023c). BettyCroft/HEMCO: 13.3.4.test4 (13.3.4.test4) [Software]. *Zenodo*. https://doi.org/10.5281/zenodo.10026844

The International GEOS-Chem User Community. (2023d). geoschem/GCHP: GCHP 14.2.0 (14.2.0) [Software]. *Zenodo*. https://doi.org/10.5281/zenodo.8411829

The International GEOS-Chem User Community. (2024). geoschem/GCHP: GCHP 14.3.0 (14.3.0) [Software]. *Zenodo*. https://doi.org/10.5281/zenodo.10640559

Twomey, S. A., Piepgrass, M., & Wolfe, T. L. (1984). An assessment of the impact of pollution on global cloud albedo. *Tellus B: Chemical and Physical Meteorology*, *36B*(5), 356–366. https://doi.org/10.1111/j.1600-0889.1984.tb00254.x

Van Der Werf, G. R., Randerson, J. T., Giglio, L., Van Leeuwen, T. T., Chen, Y., Rogers, B. M., et al. (2017). Global fire emissions estimates during 1997-2016. *Earth System Science Data*, *9*(2), 697–720. https://doi.org/10.5194/essd-9-697-2017

Vehkamaki, H., Kulmala, M., Napari, I., Lehtinen, K. E. J., Timmreck, C., Noppel, M., & Laaksonen, A. (2002). An improved parameterization for sulfuric acid—Water nucleation rates for tropospheric and stratospheric conditions. *Journal of Geophysical Research*, *107*(D22), 4622. https://doi.org/10.1029/2002JD002184

Wainwright, C. D., Pierce, J. R., Liggio, J., Strawbridge, K. B., Macdonald, A. M., & Leaitch, R. W. (2012). The effect of model spatial resolution on secondary organic aerosol predictions: A case study at Whistler, BC, Canada. *Atmospheric Chemistry and Physics*, *12*(22), 10911–10923. https://doi.org/10.5194/acp-12-10911-2012

Wang, Q., Jacob, D. J., Fisher, J. A., Mao, J., Leibensperger, E. M., Carouge, C. C., et al. (2011). Sources of carbonaceous aerosols and deposited black carbon in the Arctic in winter-spring: Implications for radiative forcing. *Atmospheric Chemistry and Physics*, *11*(23), 12453–12473. https://doi.org/10.5194/acp-11-12453-2011

Wang, Q., Jacob, D. J., Spackman, J. R., Perring, A. E., Schwarz, J. P., Moteki, N., et al. (2014). Global budget and radiative forcing of black carbon aerosol: Constraints from pole-to-pole (HIPPO) observations across the Pacific. *Journal of Geophysical Research: Atmospheres*, *119*(1), 195–206. https://doi.org/10.1002/2013JD020824

Weng, H., Lin, J., Martin, R., Millet, D. B., Jaeglé, L., Ridley, D., et al. (2020). Global high-resolution emissions of soil NOx, sea salt aerosols, and biogenic volatile organic compounds. *Scientific Data*, *7*(1), 148. https://doi.org/10.1038/s41597-020-0488-5

Wesely, M. L. (1989). Parameterization of surface resistances to gaseous dry deposition in regional-scale numerical models. *Atmospheric Environment*, *23*(6), 1293–1304. https://doi.org/10.1016/0004-6981(89)90153-4

Westervelt, D. M., Pierce, J. R., Riipinen, I., Trivitayanurak, W., Hamed, A., Kulmala, M., et al. (2013). Formation and growth of nucleated particles into cloud condensation nuclei: Model–measurement comparison. *Atmospheric Chemistry and Physics*, *13*(15), 7645–7663. https://doi.org/10.5194/acp-13-7645-2013

Williamson, C. J., Kupc, A., Axisa, D., Bilsback, K. R., Bui, T., Campuzano-Jost, P., et al. (2019). A large source of cloud condensation nuclei from new particle formation in the tropics. *Nature*, *574*(7778), 399–403. https://doi.org/10.1038/s41586-019-1638-9

Yu, F., & Luo, G. (2009). Simulation of particle size distribution with a global aerosol model: Contribution of nucleation to aerosol and CCN number concentrations. *Atmospheric Chemistry and Physics*, *9*(20), 7691–7710. https://doi.org/10.5194/acp-9-7691-2009

Yu, K., Keller, C. A., Jacob, D. J., Molod, A. M., Eastham, S. D., & Long, M. S. (2018). Errors and improvements in the use of archived meteorological data for chemical transport modeling: An analysis using GEOS-Chem v11-01 driven by GEOS-5 meteorology. *Geoscientific Model Development*, *11*(1), 305–319. https://doi.org/10.5194/gmd-11-305-2018

Zaidan, M. A., Haapasilta, V., Relan, R., Paasonen, P., Kerminen, V.-M., Junninen, H., et al. (2018). Exploring non-linear associations between atmospheric new-particle formation and ambient variables: A mutual information approach. *Atmospheric Chemistry and Physics*, *18*(17), 12699–12714. https://doi.org/10.5194/acp-18-12699-2018

Zakoura, M., & Pandis, S. N. (2018). Overprediction of aerosol nitrate by chemical transport models: The role of grid resolution. *Atmospheric Environment*, *187*, 390–400. https://doi.org/10.1016/j.atmosenv.2018.05.066

Zaveri, R. A., Easter, R. C., Singh, B., Wang, H., Lu, Z., Tilmes, S., et al. (2021). Development and evaluation of chemistry-aerosol-climate model CAM5-Chem-MAM7-MOSAIC: Global atmospheric distribution and radiative effects of nitrate aerosol. *Journal of Advances in Modeling Earth Systems*, *13*(4). https://doi.org/10.1029/2020MS002346

Zender, C. S., Bian, H., & Newman, D. (2003). Mineral dust entrainment and deposition (DEAD) model: Description and 1990s dust climatology. *Journal of Geophysical Research*, *108*(D14), 4416. https://doi.org/10.1029/2002JD002775

Zhang, D., Martin, R. V., Bindle, L., Li, C., Eastham, S. D., van Donkelaar, A., & Gallardo, L. (2023). Advances in simulating the global spatial heterogeneity of air quality and source sector contributions: Insights into the global South. *Environmental Science & Technology*, *57*(17), 6955–6964. https://doi.org/10.1021/acs.est.2c07253

Zhang, L., Liu, L., Zhao, Y., Gong, S., Zhang, X., Henze, D. K., et al. (2015). Source attribution of particulate matter pollution over North China with the adjoint method. *Environmental Research Letters*, *10*(8), 084011. https://doi.org/10.1088/1748-9326/10/8/084011

Zheng, G., Wang, Y., Aiken, A. C., Gallo, F., Jensen, M. P., Kollias, P., et al. (2018). Marine boundary layer aerosol in the eastern North Atlantic: Seasonal variations and key controlling processes. *Atmospheric Chemistry and Physics*, *18*(23), 17615–17635. https://doi.org/10.5194/acp-18-17615-2018

Zhu, H., Martin, R. V., Croft, B., Zhai, S., Li, C., Bindle, L., et al. (2023). Parameterization of size of organic and secondary inorganic aerosol for efficient representation of global aerosol optical properties. *Atmospheric Chemistry and Physics*, *23*(9), 5023–5042. https://doi.org/10.5194/acp-23-5023-2023

Zhuang, J., Jacob, D. J., & Eastham, S. D. (2018). The importance of vertical resolution in the free troposphere for modeling intercontinental plumes. *Atmospheric Chemistry and Physics*, *18*(8), 6039–6055. https://doi.org/10.5194/acp-18-6039-2018

Zhuang, J., Jacob, D. J., Lin, H., Lundgren, E. W., Yantosca, R. M., Gaya, J. F., et al. (2020). Enabling high-performance cloud computing for Earth science modeling on over a thousand cores: Application to the GEOS-Chem atmospheric chemistry model. *Journal of Advances in Modeling Earth Systems*, *12*(5). https://doi.org/10.1029/2020MS002064